THE STRUCTURE OF THE COMA CLUSTER OF GALAXIES

Thesis by

Thomas Wyatt Noonan

In Partial Fulfillment of the Requirements

For the Degree of

Doctor of Philosophy

California Institute of Technology

Pasadena, California

1961

ACKNOWLEDGMENTS

The writer wishes to thank Dr. H. P. Robertson for encouragement and assistance in pursuing this study, Drs. Allan Sandage and George Abell for encouragement and assistance in the observational section, and Drs. Abell and Mayall for the use of their unpublished data.

The writer expresses his gratitude for financial assistance provided by the Woodrow Wilson Foundation and the California Institute of Technology.

ABSTRACT

In a re-interpretation of Zwicky's Coma-cluster counts, the brighter and fainter galaxies have nearly identical distributions, and the cluster covers an area approximately 3°20' in diameter. There are approximately 1560 members to the limit of the 48-inch Schmidt telescope. Zwicky's data are consistent with a recent survey of the Coma cluster by Abell.

The observed counts closely resemble the distribution of matter in an isothermal gas sphere. Any method for computing the mass which uses the structure of the isothermal gas sphere is equivalent to applying the virial theorem. The virial-theorem mass based on latest available data is $2 \times 10^{15} M_{\odot}$.

It is not difficult for a non-equilibrium model to have a distribution similar to the isothermal gas sphere. The hypothesis that the Coma cluster is a young cluster is consistent with the observed spatial distribution and colors of the galaxies. The age could be as short as 2×10^{9} years, and the "hidden mass" could be in the unseen parts of galaxies still evolving.

CONTENTS

INTRODUCTION

THE PROBLEM OF THE COMA CLUSTER

Some of the galaxies in the sky which can be observed by means of telescopes are found in groups of various sizes ranging from two galaxies to hundreds of galaxies. With the assumption that such an assembly of galaxies is a physical system which has existed for an appreciable time in much the same form as we find it, its mass can be estimated by means of dynamical methods of physics. It is found in general that the masses so estimated are many times larger than what one would expect on the basis of the masses of single galaxies as determined by motions within the galaxy itself. Efforts have been made to resolve this discrepancy by looking in either of two directions for the solution: (1) there is unseen mass in these groups, perhaps in the form of intergalactic gas; (2) the groups are not in the steady state assumed for the calculation. Most clusters of galaxies are irregular enough in appearance that the non-equilibrium explanation seems plausible. However, the Coma cluster of galaxies stands out as an example of a very spherical-appearing cluster for which the non-equilibrium hypothesis seems implausible. Yet there is insufficient evidence to conclude that there is enough intergalactic

matter in this cluster to resolve the discrepancy.[1]

The Coma cluster is located at right ascension $12^h\ 56^m.5$ and declination 28° 13' (1950) [2] and contains at least 1560 members distributed over an area approximately 3° 20' in diameter. The brightest galaxy has a photographic magnitude of 12.4. Going to magnitudes 13.0, 14.0, 15.0, and 16.0 includes respectively the 2, 20, 100, and 200 brightest galaxies in the cluster.

The purpose of this thesis is to (1) present a new interpretation of some observational data, (2) review the mass problem, and (3) suggest a different approach.

THE PROJECTED-DISTRIBUTION FUNCTION

We are dealing with a cluster of objects with a spherically symmetric distribution. We only observe their spatial distribution as it is projected to us on the plane of the sky. The spatial density $\rho(r)$ of the objects must be inferred from their projected density $\zeta(r)$:

$$\rho(r) = -\frac{1}{\pi}\int_r^\infty \frac{1}{\sqrt{r'^2-r^2}}\,\frac{d\,\zeta(r')}{dr'}\,dr' \ .$$

($\underline{r}$ will be used somewhat ambiguously to denote both the projected radius and the spatial radius from the center of the cluster.) In our treatment,

however, we will in principle be comparing the projected densities of various models with the observed projected density. For a model having spatial density $\rho(r)$, the projected density is

$$\zeta(r) = 2\int_r^\infty \frac{\rho(r')\, r'\, dr'}{\sqrt{r'^2 - r^2}} .$$

The projected-distribution function $F(r)$ is calculated from the projected density:

$$F(r) = \frac{\int_0^r 2\pi r'^2\, \zeta(r')\, dr'}{\int_0^\infty 2\pi r'^2\, \zeta(r')\, dr'} .$$

$F(r)$ is the fraction of objects that appear within a circle of radius r.

MODEL A

A particular distribution of matter to be used extensively is model A in which the density (of objects or of mass) is given by

$$\rho(r) = \frac{b}{c^2} \qquad 0 < r < c ,$$

$$\rho(r) = \frac{b}{r^2} \qquad c < r < R ,$$

$$\rho(r) = 0 \qquad R < r .$$

The total quantity of matter, whether number of objects or mass, is

$$4\pi b(R - \tfrac{2}{3}c) \ .$$

When normalization is desired, as in the computation of the projected-distribution function $F(r)$, the total quantity is set equal to unity. For $c < r < R$,

$$1 - F(r) = \frac{1}{1 - \frac{2}{3}\frac{c}{R}}\left[\sqrt{1 - \frac{r^2}{R^2}} - \frac{r}{R}\cos^{-1}\frac{r}{R}\right] .$$

It is not important to know $F(r)$ in the region $0 < r < c$ because c will usually be small.

The case $c = 0$ will prove to be extremely useful; it will be designated model A_0:

$$\rho(r) = \frac{b}{r^2} \qquad 0 < r < R \ ,$$
$$\rho(r) = 0 \qquad R < r \ .$$

PART I. OBSERVATIONS

VELOCITIES

The only way to determine the motion of a galaxy is by the Doppler shift of the light reaching us from it. This method gives the component of the galaxy's velocity parallel to the direction from the galaxy to us. Although there is some question as to how much of the redshift of distant galaxies is possibly due to some cosmological phenomenon as yet unknown,[3] this problem is eliminated if we consider motions of the galaxies in a compact cluster relative to the cluster itself. Thus the velocity of a galaxy relative to the cluster is given by

$$v = c\left[\left(\frac{\Delta\lambda}{\lambda}\right)_{\text{galaxy}} - \left(\frac{\Delta\lambda}{\lambda}\right)_{\text{mean for cluster}}\right].$$

$\underline{v}$ will be used for line-of-sight velocity and $\underline{w}$ will be used for actual velocity. Also, as a convention, $c\frac{\Delta\lambda}{\lambda}$ will be called the "recessional velocity".

Dr. Mayall at the Lick Observatory has kindly made available to me the redshift data for 28 galaxies in addition to the data for 22 galaxies taken at Mount Wilson. Of these 50 galaxies, 9 lie beyond the 100' radius of the cluster, and another has a recessional velocity of less than 3000 km/sec. The remaining 40 galaxies are assumed to belong to

the cluster.

The mean velocity of recession is 6850 km/sec, and the root-mean-square deviation from this mean is 1050 km/sec, with some members differing from the mean by as much as 2500 km/sec. Based on this mean and Sandage's[4] distance scale of 75 $\frac{\text{km}}{\text{sec-Mpc}}$, the distance to the Coma cluster is 90 Mpc. This distance will be assumed throughout this thesis. The radius $\underline{R}$ of the cluster is taken to be 100' or 2.62 Mpc.

A plot of the 40 galaxies in the $\underline{v}$-$\underline{r}$ plane gives the histogram shown in figure 1. The $\underline{v}$-$\underline{r}$ distributions for three models have been calculated (app. I): (A) a pure explosion, (B) the galaxies moving in circular orbits randomly oriented, and (C) model B to be described in part III. The distributions are shown in figures 2, 3, and 4, respectively, where the third dimension represents the density in $\underline{v}$-$\underline{r}$ space. Due to the fewness of the galaxies whose redshifts have been observed, the only conclusion to be drawn is that the Coma cluster can fit any of these models.

FIELD GALAXIES

In making counts of galaxies in a cluster of galaxies, whether for their distribution in space or their distribution in luminosity, there are

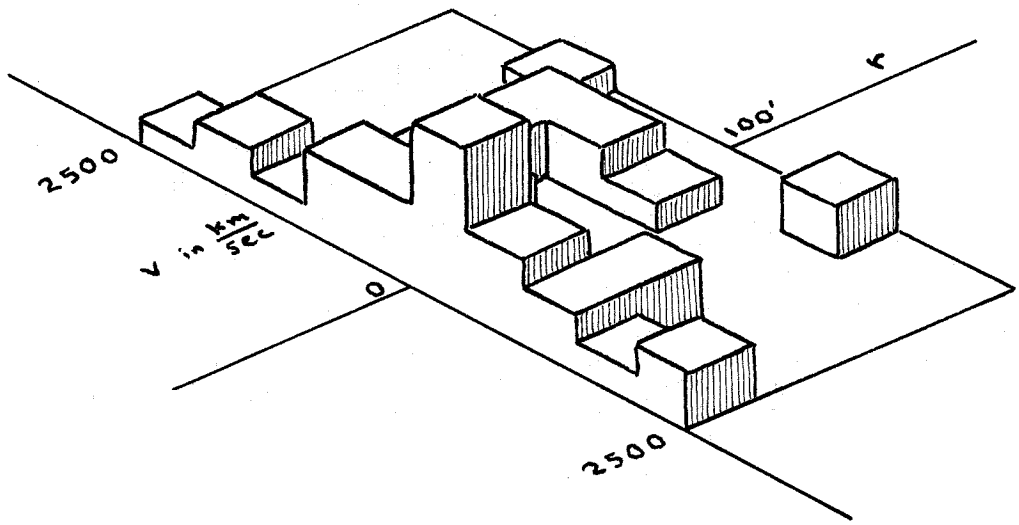

FIGURE 1

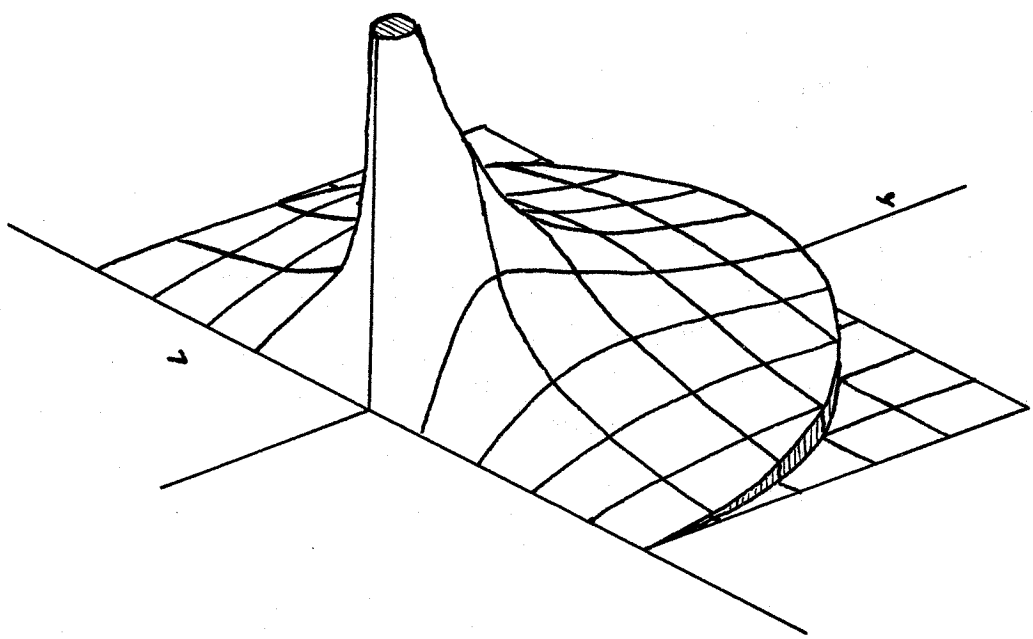

FIGURE 2

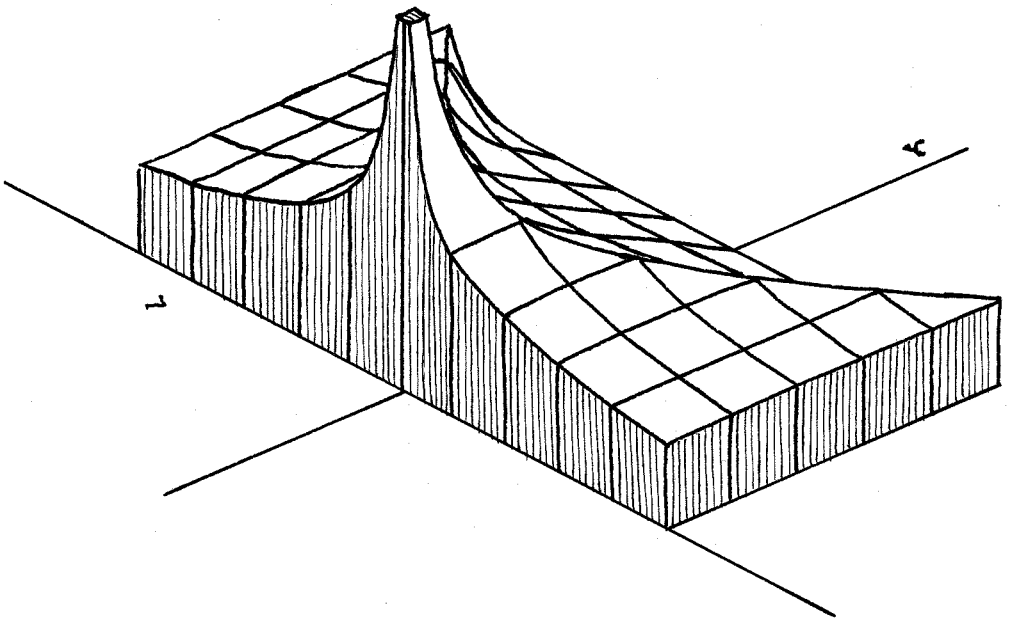

FIGURE 3

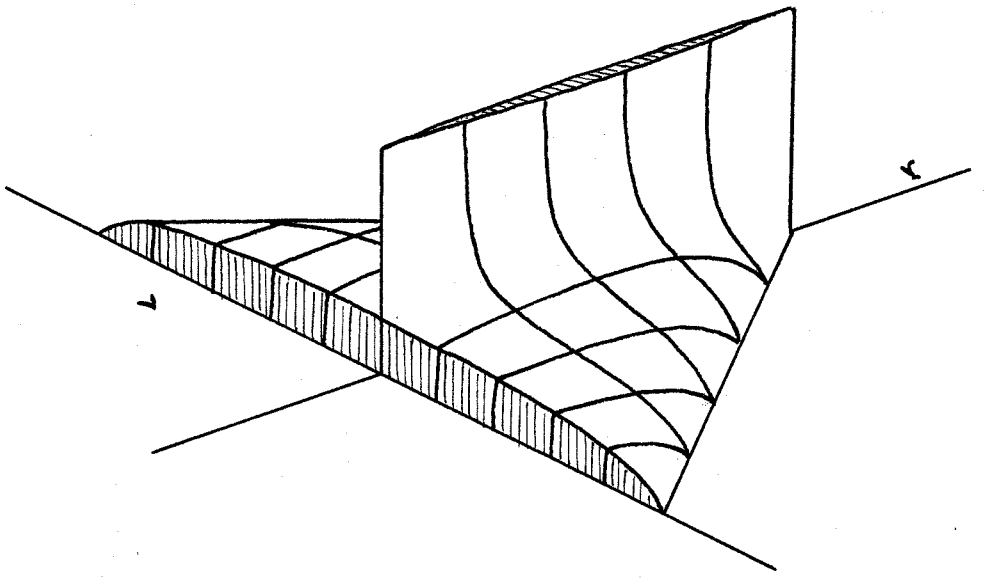

FIGURE 4

background galaxies called field galaxies which are included in the counting. The number of these galaxies must be estimated and subtracted out in order to obtain data representing the cluster alone. It will be assumed that the field galaxies in the region of the Coma cluster are uniformly distributed in space with a luminosity function which is independent of position, and that they are visible without obscuration. Then it follows that the field galaxies brighter than an apparent photographic magnitude $\underline{m}$ have a uniform density $n_f(m)$ per square degree given by

$$\log n_f(m) = 0.6m - C \ , \qquad (1)$$

where $\underline{C}$ is a constant to be determined by observation. Hubble[5] found that if $n_f(m)$ represents an average over the whole sky, then $C = 9.10$. However, we do not expect that for the region of the Coma cluster $\underline{C}$ should have exactly this same value because of possible large-scale variations in the distribution of field galaxies across the sky. Also, there were errors in Hubble's magnitude estimates.

ZWICKY'S COUNTS

Introduction

Zwicky's counts will be used to determine the spatial distribution of galaxies in the Coma cluster. He made counts in concentric rings centered on the cluster on plates obtained with the 18-inch Schmidt telescope at Palomar,[6,7] and later with the 48-inch Schmidt telescope.[7,8]

He used two methods to estimate the density of field galaxies on his plates: (a) the average density of galaxies in regions of lowest density (extrapolated in the case of the 18-inch counts); and (b) as given by equation 1. His estimates of the limiting magnitudes for his 18-inch and 48-inch plates were 16.5 and 19.0, respectively. He estimated the densities to be 7.38 deg^{-2} and 170 deg^{-2} by method (a) and demonstrated that these densities are consistent with method (b) for Hubble's value of C.

Zwicky concluded: (a) the cluster galaxies in the 18-inch plates extend to at least a radius of 160', and there are 639 of them within this radius; and (b) the cluster galaxies in the 48-inch plates extend further than 6° from the center of the cluster, and there are 10724 of them within this radius. Conclusions regarding the distribution of faint galaxies in the cluster are very sensitive to

the estimate of the density of field galaxies. We will assume a different density than Zwicky used.

The following notation will be used in part I.

18-inch	48-inch	
m_1	m_2	= the limiting magnitude.
$n_f(m_1)$	$n_f(m_2)$	= the number of field galaxies per square degree.
a_1	a_2	= π times the number of field galaxies per square minute.
$N_1(r)$	$N_2(r)$	= the number of galaxies within a projected circle of radius r, centered on the cluster, i.e., the accumulative sum of Zwicky's ring counts.
$N_1'(r)$	$N_2'(r)$	= the number of cluster galaxies within a circle of radius r.
$\mathcal{N}_1$	$\mathcal{N}_2$	= the total number of cluster galaxies.

From these definitions it follows that

$$N_1'(r) = N_1(r) - a_1 r^2 \ , \quad N_2'(r) = N_2(r) - a_2 r^2 .$$

The 48-inch Counts

When $N_2(r)$ is plotted as a function of r^2 (fig. 5), the portion of the curve between 100' and 250' appears to be nearly straight. We will assume that this is the line $\mathcal{N}_2 + a_2 r^2$. The slope is

TABLE 1. ZWICKY'S COUNTS

r		$N_2(r)$	a_2r^2	$N_2'(r)$	$F_2(r)$	$\frac{r^2}{N_2'}$
2'.5						
5'	60	60	6	54	0.035	0.46
10	125	185	24	161	.103	0.62
15	152	337	54	283	.181	0.80
20	166	503	96	407	.261	0.98
25	151	654	150	504	.323	1.24
30	174	828	216	612	.392	1.47
35	183	1011	294	717	.460	1.71
40	182	1193	384	809	.519	1.98
45	177	1370	486	884	.567	2.29
50	218	1588	600	988	.633	2.53
55	204	1792	726	1066	.683	2.84
60	252	2044	864	1180	.756	3.05
70	453	2497	1176	1321	.847	3.71
80	471	2968	1536	1432	.918	4.47
90	441	3409	1944	1465	.939	5.53
100	530	3939	2400	1539	.987	6.50
110	508	4447	2904	1543	.989	7.84
120	583	5030	3456	1574	1.009	9.15
130	653	5683	4056	1627	1.043	10.39
140	658	6341	4704	1637	1.049	11.97
150	638	6979	5400	1579	1.012	14.25
160	709	7688	6144	1544	.990	16.58
170	736	8424	6936	1488		
180	843	9267	7776	1491		
190	875	10142	8664	1478		
200	953	11095	9600	1495		
210	1108	12203	10584	1619		
220	992	13195	11616	1579		
230	1024	14219	12696	1523		
240	1209	15428	13824	1604		
270	3436	18864	17496	1368		
300	3466	22330	21600	730		
330	3629	25959	26136	-177		
360	3992	29951	31104	-1153		

TABLE 1. (cont.)

r		N_1	$a_1 r^2$	N_1'	F_1	$\frac{N_1}{N_2'}$	η
2'5	15	15	0	15	0.027		
5'	16	31	0	31	.056	0.574	0.573
10	42	73	1	72	.129	.453	.445
15	53	126	2	124	.223	.445	.440
20	44	170	4	166	.298	.418	.407
25	39	209	6	203	.364	.415	.403
30	48	257	9	248	.445	.420	.406
35	25	282	12	270	.485	.393	.377
40	41	323	15	308	.553	.399	.381
45	31	354	19	335	.601	.400	.379
50	41	395	24	371	.666	.400	.376
55	37	432	28	404	.725	.405	.378
60	36	468	34	434	.779	.397	.368
65	29	497	40	457	.820		
70	40	537	47	490	.880	.407	.371
75	19	556	53	503	.903		
80	15	571	60	511	.917	.399	.357
85	17	588	69	519	.932		
90	15	603	76	527	.946	.412	.359
95	16	619	85	534	.959		
100	25	644	94	550	.987	.418	.358
110	24	668	114	554	.995	.433	.358
120	37	705	136	569	1.022	.448	.362
130	31	736	160	576	1.034	.452	.354
140	18	754	185	569	1.022	.461	.348
150	30	784	212	572	1.027	.497	.362
160	20	804	242	562	1.009	.521	.364

The ring counts are given in the unlabeled columns.

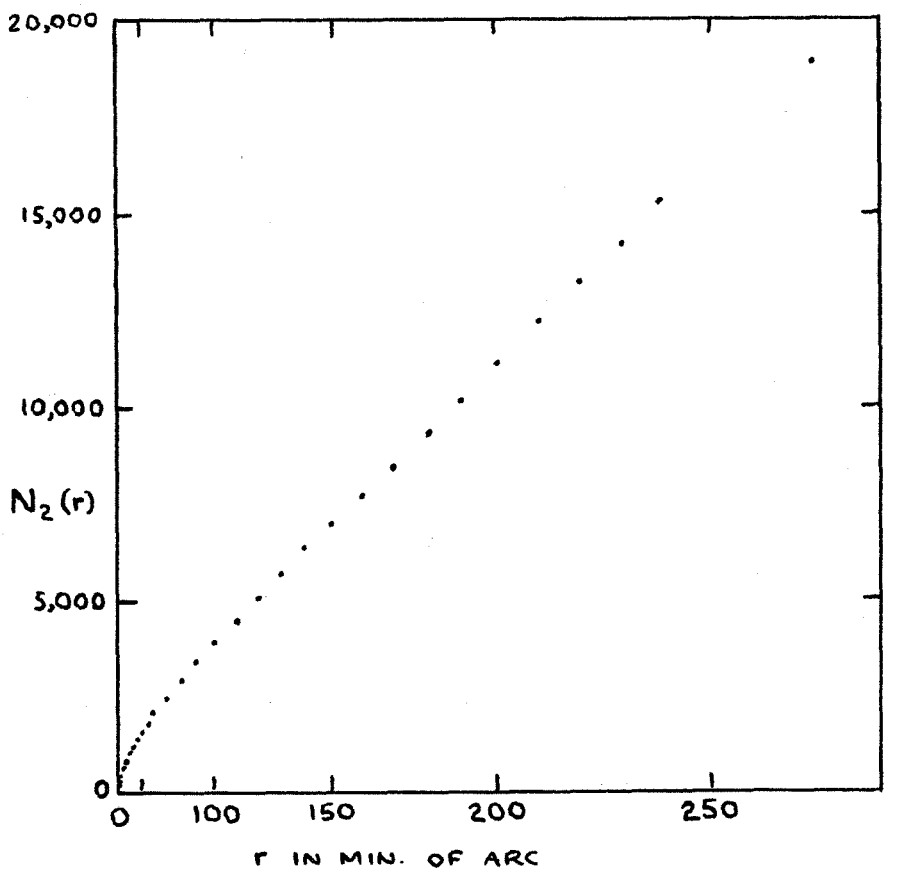

FIGURE 5

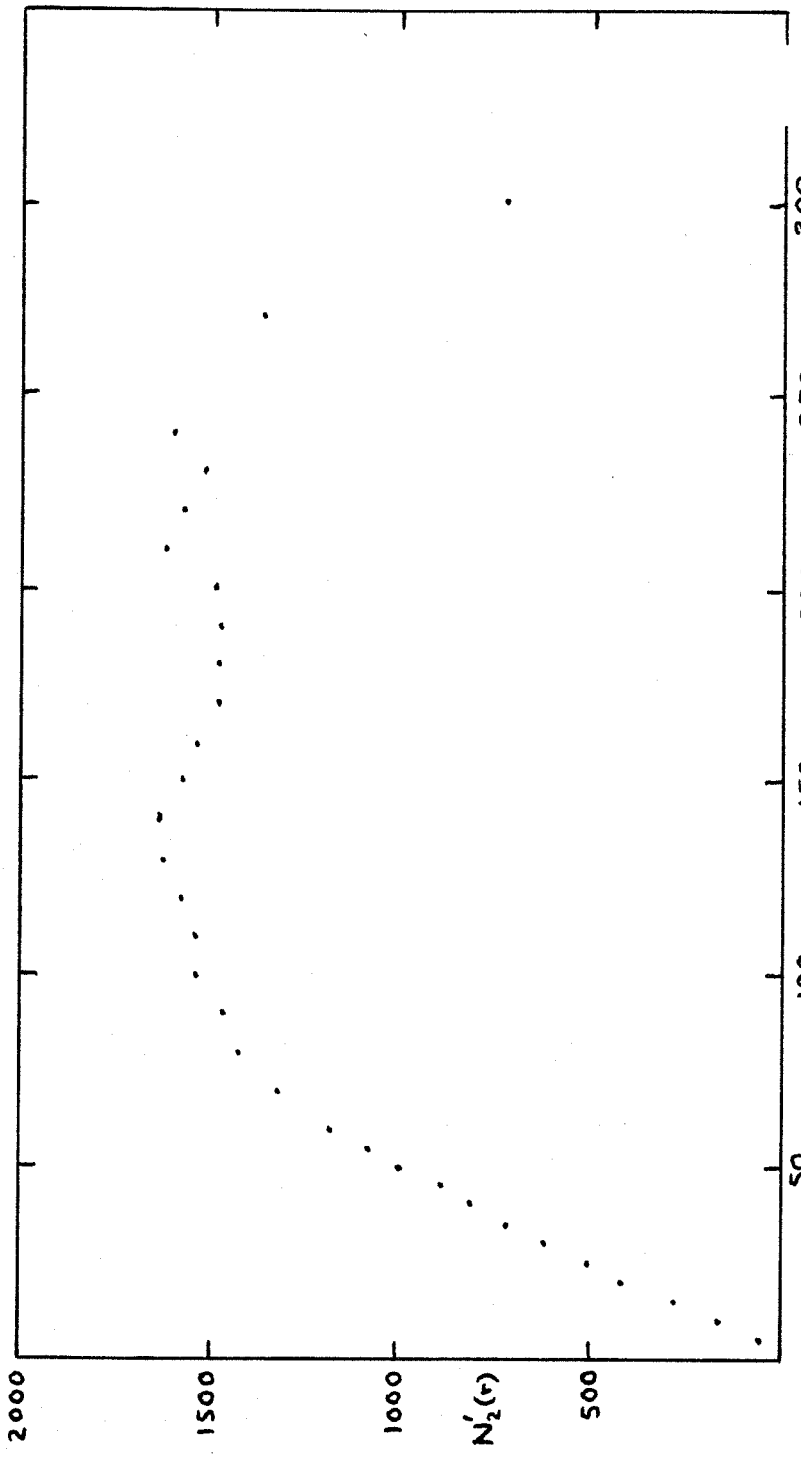

FIGURE 6

$$a_2 = 0.240 \pm 0.002 \text{ min}^{-2}$$

or $$n_f(m_2) = 275 \pm 2 \text{ deg}^{-2}.$$

(The limits indicate the assumed maximum range of uncertainty in the present analysis.) $N_2'(r)$ rises for the first 100' (fig. 6) and then levels off at a value of approximately 1560. We conclude that

$$\mathcal{N}_2 = 1560 \pm 40 ,$$

and that the radius of the cluster is approximately 100'. The dip in $N_2'(r)$ beyond 250' is probably due to variations in the field density as shown in the survey by Shane and Wirtanen.[9]

The 18-inch Counts

Consider now the ratio $\eta(r)$ of the brighter cluster galaxies (with magnitudes less than m_1) to the fainter cluster galaxies (with magnitudes less than m_2) within a circle of radius r:

$$\eta(r) = \frac{N_1(r) - a_1 r^2}{N_2'(r)} .$$

We found that the cluster does not extend appreciably beyond 100', so that $\eta(r)$ should be constant for $r > 100'$. Therefore $N_1(r)/N_2'(r)$ when plotted against $r^2/N_2'(r)$ should show a straight line in the region $r > 100'$ with slope a_1 (fig. 7). This

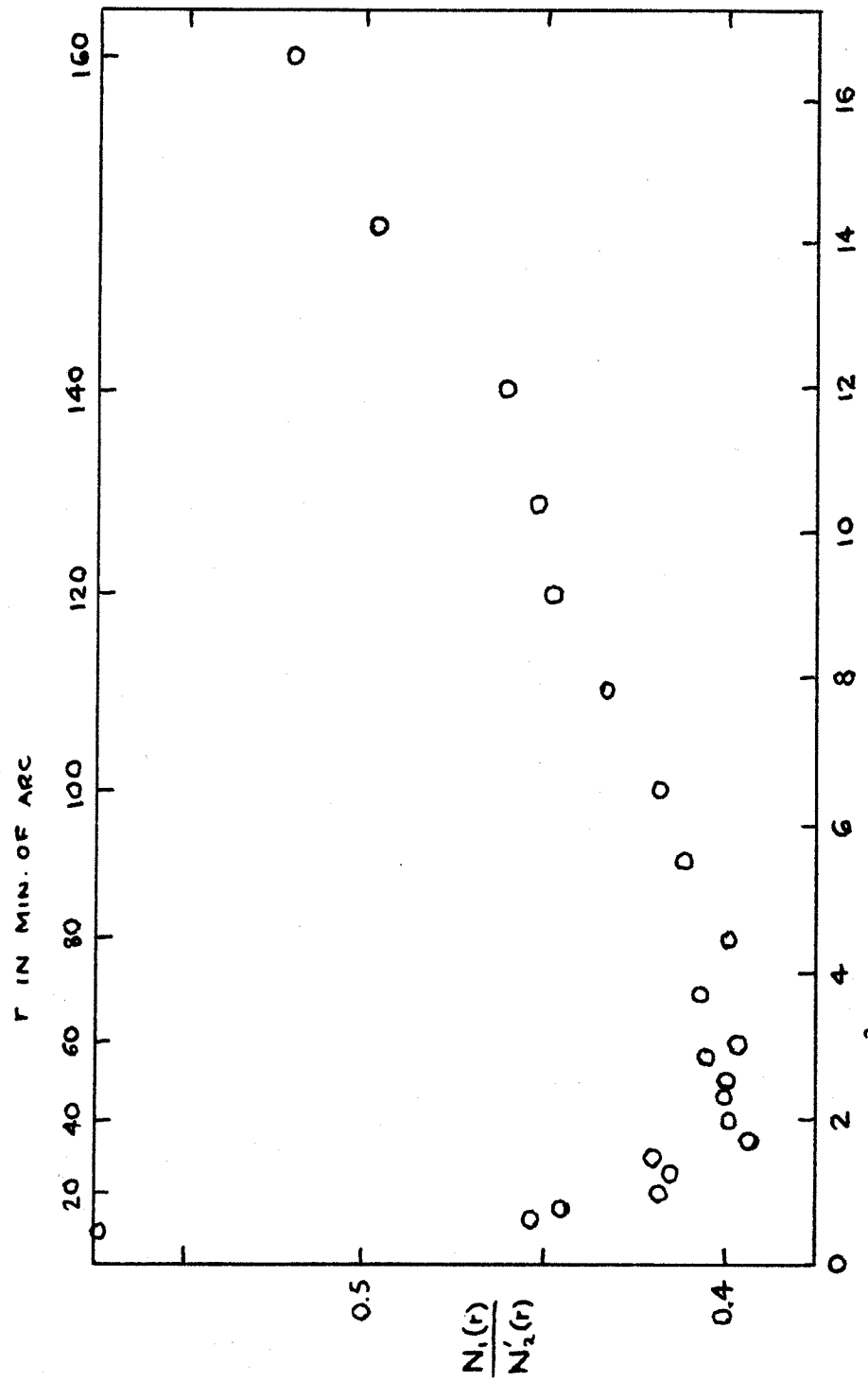
r IN MIN. OF ARC
20
40
60
80
100
120
140
160
0.5
0.4
$\frac{N_1(r)}{N_2'(r)}$
0
2
4
6
8
10
12
14
16
$\frac{r^2}{N_2'(r)}$ IN MIN²

FIGURE 7

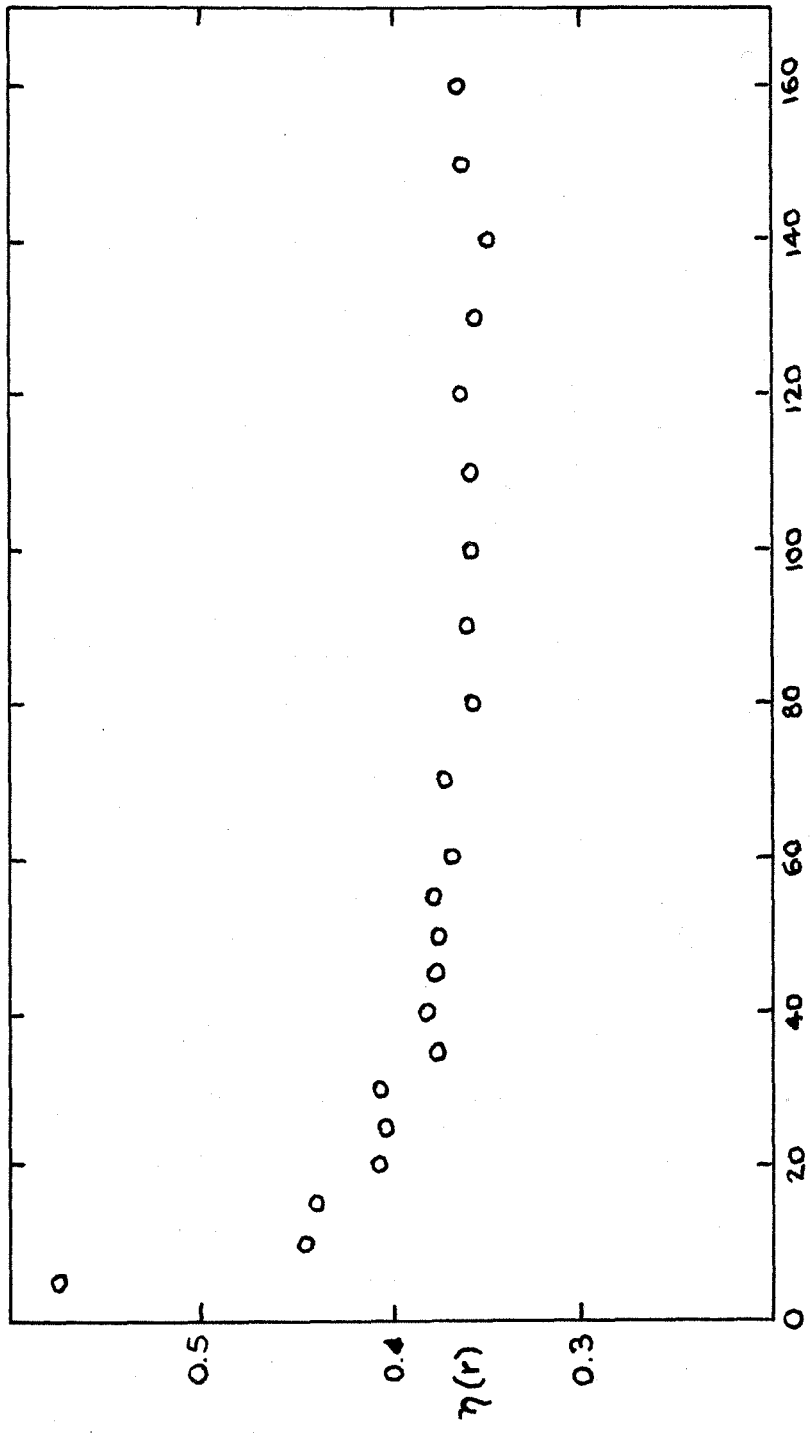

FIGURE 8

appears to be very nearly the case. The slope of the straight part which extends from 80' is

$$a_1 = 0.0095 \pm 0.0020 \text{ min}^{-2}$$

or

$$n_f(m_1) = 11 \pm 2 \text{ deg}^{-2} .$$

With this value of a_1, $\eta(r)$ is constant for $r > 80'$ at a value of 0.357 ± 0.008 (fig. 8). Therefore

$$\mathcal{N}_1 = (0.357 \pm 0.008)(1560 \pm 40)$$

or

$$\mathcal{N}_1 = 557 \pm 27 .$$

Comparison of the 18-inch and 48-inch Counts

The distributions of the brighter and fainter galaxies can now be compared. We define

$$F_1(r) = \frac{N_1'(r)}{\mathcal{N}_1} \quad \text{and} \quad F_2(r) = \frac{N_2'(r)}{\mathcal{N}_2} ,$$

which are plotted in figures 9 and 13. It is seen that the two distributions are nearly identical. The $F_1(r)$ points appear to be shifted approximately 2'.5 to the left of the $F_2(r)$ points. If this effect is real, it indicates that the brighter galaxies are slightly more centrally located than the fainter ones.

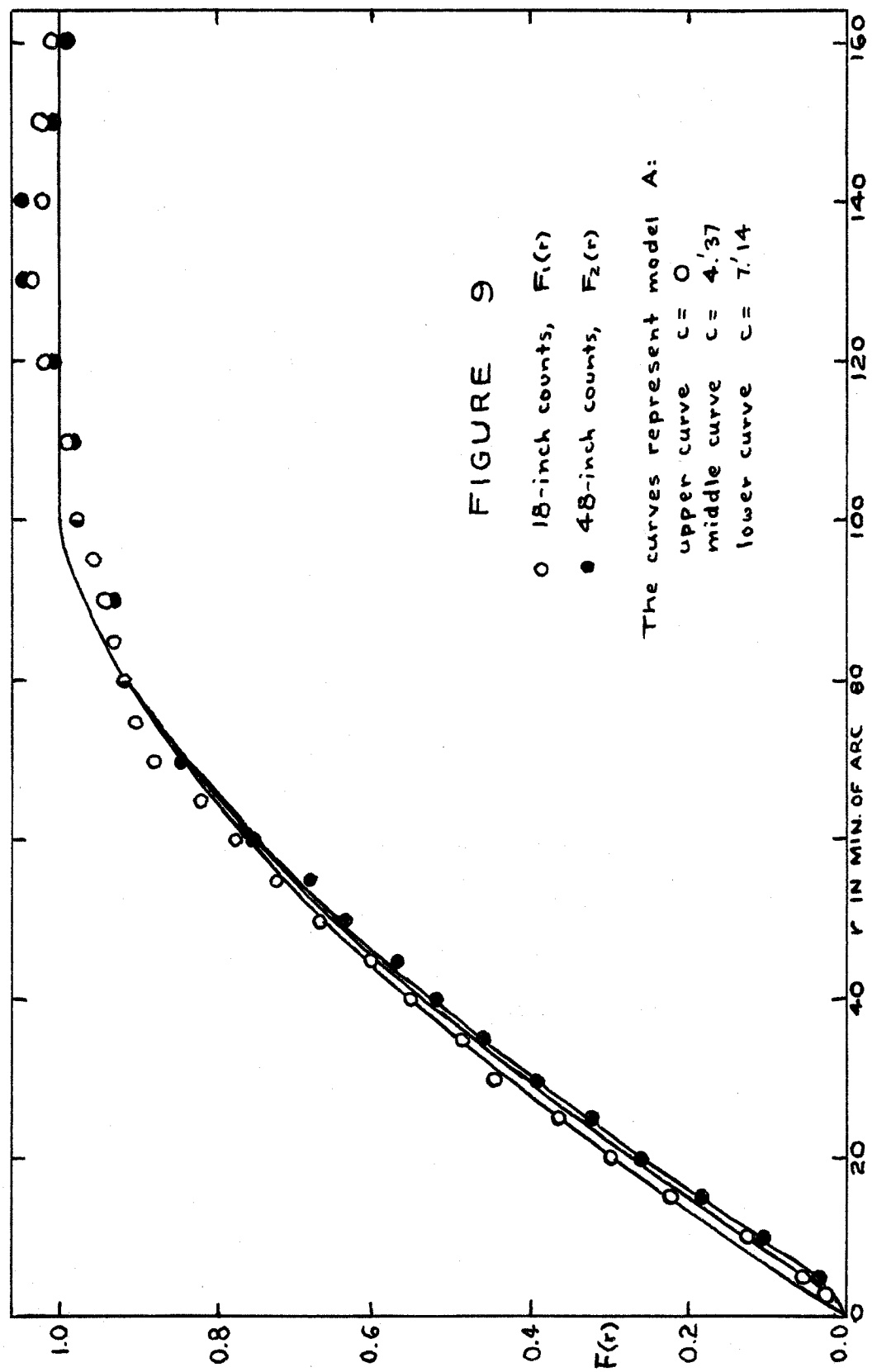
FIGURE 9
o 18-inch counts, $F_1(r)$
• 48-inch counts, $F_2(r)$
The curves represent model A:
upper curve c = 0
middle curve c = 4.'37
lower curve c = 7.'14
F(r)
r IN MIN. OF ARC
0.0
0.2
0.4
0.6
0.8
1.0
0
20
40
80
100
120
140
160

THE LUMINOSITY FUNCTION

Abell[10] has recently investigated the Coma cluster both for the spatial distribution and the luminosity function of its member galaxies. He used the 48-inch Schmidt telescope for the survey, and calibrated the magnitudes photoelectrically with the 100-inch telescope at Mount Wilson. His survey covers a region 156' by 162' with area

$$A = 7.03 \pm 0.04 \text{ deg}^2$$

centered on the cluster. He observed 1722 galaxies to a limiting photographic magnitude of 19.4 ± 0.3. He estimated that 705 of them are field galaxies.

Only a fraction $\underline{f}$ of the cluster galaxies are included to any given magnitude limit, because his field does not include the entire cluster. A numerical integration based on $F_2(r)$ gives a value

$$f = 0.942 \pm 0.013 ,$$

while a determination based on model A gives

$$f = 0.958$$

(app. II). We will adopt

$$f = 0.940 \pm 0.015 .$$

A comparison of Zwicky's data with Abell's data is given in table 2. Entries not already given are

computed by means of the operations indicated in the column headings, with the exception of the first column. The point on Abell's photographic magnitude

TABLE 2.

COMPARISON OF ZWICKY'S DATA WITH ABELL'S DATA

m_{pg}	Number of galaxies in 156' by 162' area			Total number of cluster galaxies $\mathcal{N}$	Density of field galaxies (deg^{-2}) n_f	Observer
	total $f\mathcal{N}+An_f$	field An_f	cluster $f\mathcal{N}$			
18.0	601±48	77±14	524±34	557±27	11±2	Zwicky
19.4	1722	705	1017	1082	100	Abell
m_2	3400±86	1933±25	1467±61	1560±40	275±2	Zwicky

scale at which the integrated luminosity function reaches 601 is $18^m.05$ (table 3). Allowing for the various uncertainties present, we adopt

$$m_1 = 18.0 \pm 0.2 \ .$$

If equation 1 is applied to the densities of field galaxies in table 2, there results for the three entries, respectively,

$$C = 9.8$$
$$C = 9.6$$
$$C = 0.6m_2 - 2.4.$$

The magnitudes are only accurate to a couple of tenths, so the first two values show no inconsistency. If the first value of $\underline{C}$ is assumed in the third case, then

$$m_2 = 20.3.$$

However, equation 1 probably does not apply to such a faint magnitude because cosmological corrections would be significant.

Zwicky's limiting magnitude estimates are too bright. In the early days of operation of the 48-inch telescope when Zwicky's counts were made, the photographic limit was thought to be about a magnitude brighter than it actually is, because of scale errors in the Mount Wilson photographic magnitude system.[11] Therefore, in spite of the larger values of $n_f(m_1)$ and $n_f(m_2)$ used here, we have obtained a value for $\underline{C}$ which is larger than Hubble's value.

Our field densities are consistent with the sky survey by Shane and Wirtanen which shows a density of around 40 to 70 galaxies deg^{-2} in the region surrounding the Coma cluster.[9] Their estimated limiting magnitude of 18.4 is probably too bright.[12]

We will adopt a value for $\underline{C}$ of 9.79. The number of field galaxies on Abell's plate brighter than photographic magnitude $\underline{m}$ is then

TABLE 3. PHOTOGRAPHIC LUMINOSITY FUNCTION

1	2	3	4
12.4	1	0	1
13.0	2	0	2
13.2	4	0	4
13.5	5	0	5
13.6	7	0	7
13.7	9	0	9
13.8	13	0	13
13.9	17	0	17
14.0	20	0	20
14.1	25	0	25
14.2	29	0	29
14.3	32	0	32
14.4	41	1	40
14.5	52	1	51
14.6	63	1	62
14.7	71	1	70
14.8	79	1	78
14.9	92	1	91
15.0	102	1	101
15.1	107	1	106
15.2	118	2	116
15.3	142	2	140
15.4	157	2	155
15.5	177	2	175
15.6	186	3	183
15.7	194	3	191
15.8	198	3	195
15.9	201	4	197
16.0	209	5	204
16.1	219	5	214
16.2	234	6	228
16.3	248	7	241
16.4	262	8	254
16.5	288	9	279
16.6	302	10	292
16.7	320	12	308
16.8	339	14	325
16.9	355	16	339
17.0	359	18	341
17.1	391	21	370
17.2	397	24	373
17.3	411	28	383
17.4	416	32	384
17.5	434	36	398
17.6	485	42	443
17.7	501	48	453
17.8	534	55	479
17.9	573	63	510
18.0	600	72	528
18.1	676	83	593
18.2	739	96	643
18.3	776	110	666
18.4	796	126	670
18.5	814	145	669
18.6	836	166	670
18.7	889	191	698
18.8	992	219	773
18.9	1080	251	829
19.0	1080	288	792
19.1	1136	331	805
19.2	1217	380	837
19.3	1413	436	977
19.4	1720	501	1219

Column 1: $m - 0^m.05$, where $\underline{m}$ is the limiting magnitude. The 0.05 will be neglected. Beyond 19.0, $\underline{m}$ may be in error by as much as 0.3.

Column 2: total number of galaxies brighter than $\underline{m}$.

Column 3: $10^{0.6(m-14.9)}$.

Column 4: $\ell_{pg}(m)$, number of cluster galaxies brighter than $\underline{m}$.

TABLE 4. PHOTOVISUAL LUMINOSITY FUNCTION

1	2	3	4
12.0	1	0	1
12.2	2	0	2
12.7	3	0	3
12.9	4	0	4
13.1	5	0	5
13.2	7	0	7
13.3	8	0	8
13.4	9	0	9
13.5	16	0	16
13.6	21	0	21
13.7	25	0	25
13.8	32	0	32
13.9	36	1	35
14.0	44	1	43
14.1	44	1	43
14.2	54	1	53
14.3	57	1	56
14.4	67	1	66
14.5	78	1	77
14.6	107	1	106
14.7	134	2	132
14.8	142	2	140
14.9	157	2	155
15.0	173	2	171
15.1	189	3	186
15.2	200	3	197
15.3	208	3	205
15.4	213	4	209
15.5	222	5	217
15.6	237	5	232
15.7	261	6	255
15.8	281	7	274
15.9	301	8	293
16.0	317	9	308
16.1	328	10	318
16.2	331	12	319
16.3	370	14	356
16.4	394	16	378
16.5	413	18	395
16.6	439	21	418
16.7	463	24	439
16.8	503	28	475
16.9	534	32	502
17.0	594	36	558
17.1	645	42	603
17.2	699	48	651
17.3	798	55	743
17.4	852	63	789
17.5	880	72	808
17.6	920	83	837
17.7	1029	96	933
17.8	1136	110	1026
17.9	1391	126	1265
18.0	1722	145	1577

Column 1: m - 0.05, where m is the limiting magnitude. The 0.05 will be neglected. Beyond 17.5, m may be in error by as much as 0.4.

Column 2: total number of galaxies brighter than m.

Column 3: $10^{0.6(m-14.4)}$.

Column 4: $\ell_{pv}(m)$, number of cluster galaxies brighter than m.

$$10^{0.6(m-14.9)}.$$

With the assumption that the field galaxies have a color index of 0.5, the number on the photovisual scale is

$$10^{0.6(m-14.4)}.$$

These numbers are subtracted from Abell's counts to give the integrated luminosity functions for the cluster galaxies (tables 3 and 4).

The integrated luminosity functions $\ell_{pg}(m)$ and $\ell_{pv}(m)$ are the numbers of galaxies brighter than photographic and photovisual magnitude $\underline{m}$, respectively. These two functions are plotted in figure 10. The slopes of the curves reach no maximum within the plate limits. This indicates that there can be any number of galaxies fainter than the plate limit. We know that in the neighborhood of photographic magnitude 20.3, the number rises to around 1500.

The total luminosity in solar units is given by the integral

$$\int 10^{-0.4(m-\Delta-m_o)}\, d\ell$$

where Δ is the distance modulus to the cluster and $\underline{m}_o$ is the absolute magnitude of the sun.*

* The absolute magnitude of the sun is assumed to be 5.43 (pg) and 4.86 (pv).(13)

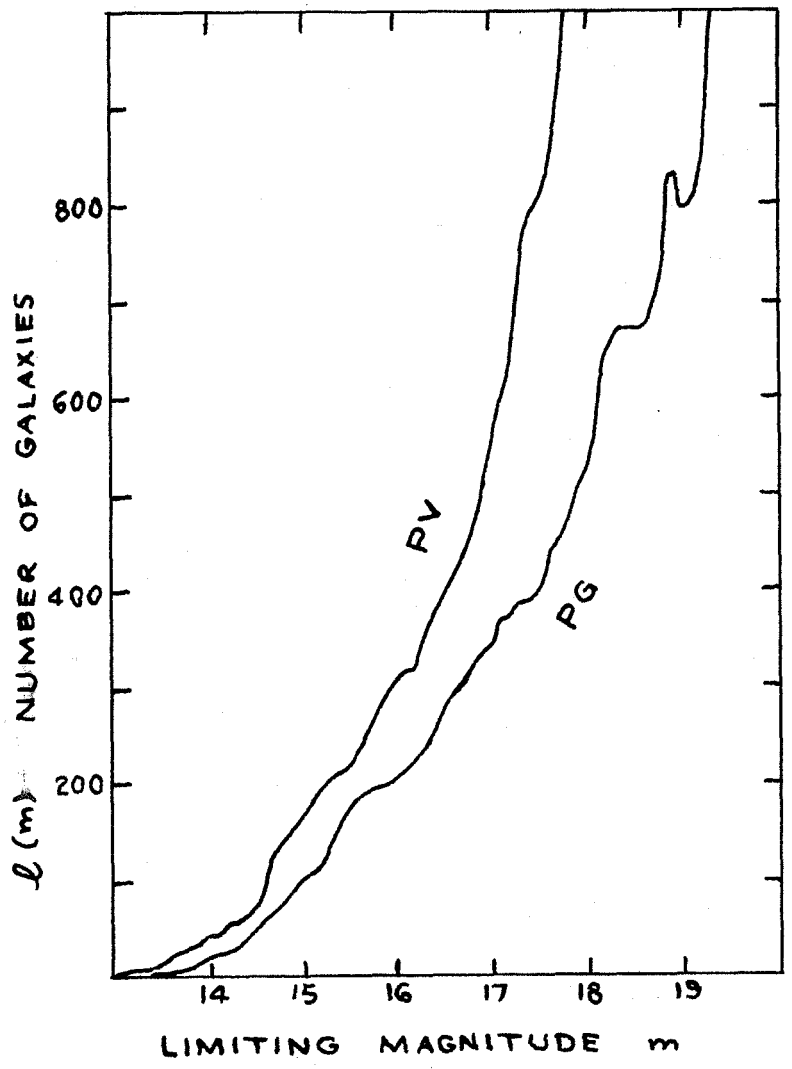
800
600
400
200
ℓ (m) NUMBER OF GALAXIES
PV
PG
14
15
16
17
18
19
LIMITING MAGNITUDE m

FIGURE 10

After dividing by f this gives

$$L_{pg} = 4.3 \times 10^{12}\ L_{\odot} \qquad L_{pv} = 4.5 \times 10^{12}\ L_{\odot}$$

for the total photographic and photovisual luminosities of the Coma cluster.

The color index of the ℓ^{th} brightest galaxy is in principle the horizontal distance between the curves in figure 10 at a height ℓ. The fainter galaxies are much redder than the brighter ones. This effect might be due to non-uniformity in Abell's magnitude sdales. However, it will be assumed that his scales are uniform.

THE L'-L DIAGRAM

The luminosity-function data will be used in the form of what we will call the L'-L diagram (fig. 11). Let L' be the photographic luminosity of a galaxy, and let L be its photovisual luminosity. A galaxy is thus represented by a point in the L'-L plane. The slope of the line from this point to the origin is proportional to $10^{-0.4\ I}$ where I is the color index of the galaxy. Pettit has measured the color indices and magnitudes of some Coma cluster galaxies;[14] their color indices vary over a range of only about 0.6, while their magnitudes vary over several magnitudes. Thus the array of points representing the Coma cluster is

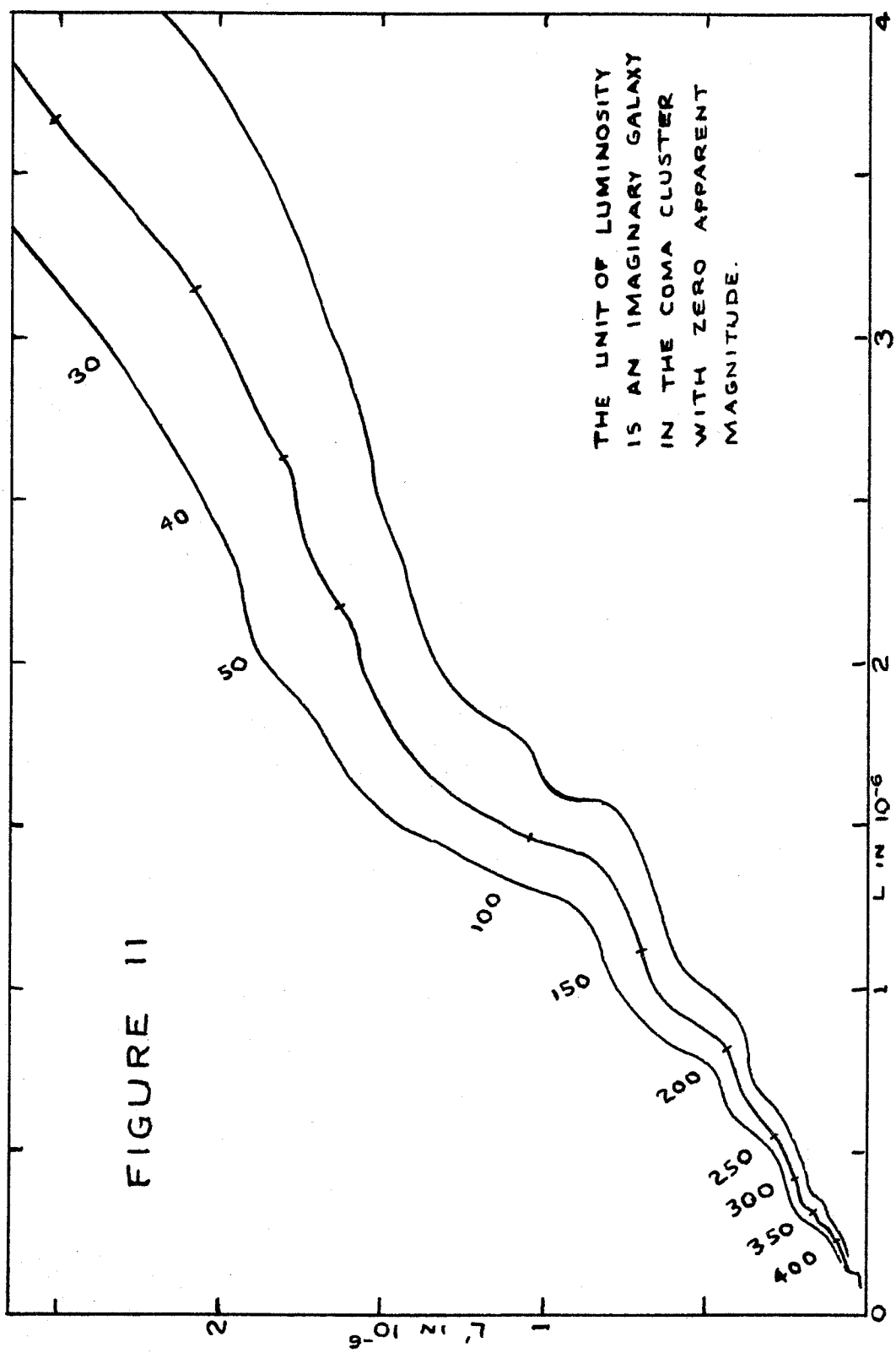
THE UNIT OF LUMINOSITY
IS AN IMAGINARY GALAXY
IN THE COMA CLUSTER
WITH ZERO APPARENT
MAGNITUDE.
30
40
50
100
150
200
250
300
350
400
L' IN 10⁻⁶
L IN 10⁻⁶
0
1
2
3
4

FIGURE 11

expected to be long and narrow. It then follows from the nature of the integrated luminosity functions $\ell_{pg}(m)$ and $\ell_{pv}(m)$ that the curve $L'(L)$ given by

$$\ell_{pg}(2.5 \log L') = \ell_{pv}(2.5 \log L)$$

runs along the middle of the array. Therefore this curve will be used to approximate the array of Coma cluster galaxies in the $\underline{L}'$-$\underline{L}$ diagram (fig. 11). $\ell_{pg} = \ell_{pv}$ is labeled along the curve. The main curve is skirted by two marginal curves which indicate the order of magnitude of counting error. The upper curve is obtained by displacing the $\ell_{pg}(m)$ curve of figure 10 $0^m.1$ to the left and the $\ell_{pv}(m)$ curve $0^m.1$ to the right; the lower curve is obtained in the corresponding opposite manner. The sharp variations in the $\underline{L}'$-$\underline{L}$ curve are due to counting errors. The broad variations are real.

An advantage of the $\underline{L}'$-$\underline{L}$ diagram is that any shifts in the zero points of the magnitude scales will only change the scales of $\underline{L}'$ and $\underline{L}$, and will not alter the basic appearance of the diagram. Also, any error in estimating the field galaxies does not appear; for large luminosities the number of field galaxies is small, and for small luminosities the curve is crowded toward the origin of the diagram so as to lose the error. The $\underline{L}'$-$\underline{L}$ diagram will be

used when considering the colors of galaxies from the point of view of theory.

ABELL'S SPATIAL DISTRIBUTION

Let us digress briefly to compare Abell's spatial distribution with Zwicky's. Abell counted in strips rather than rings. Therefore model A is used in order to compare the strip counts (fig. 12) with Zwicky's counts. The model is chosen both for its simplicity and for its close agreement with Zwicky's data. The parameter c is taken to be 4'.37. The curves in figures 9 and 12 represent the model by ring count and strip count, respectively. The curve in figure 12 is for 1082 cluster galaxies, and 25 field galaxies per strip.

It may be concluded that Abell's data is consistent with Zwicky's data. Abell also found that the spatial distributions of galaxies of different magnitude ranges do not differ appreciably from each other.

SUMMARY

At least 1560 galaxies are situated in a region approximately 100' in radius. There are many more faint galaxies than bright ones, and there may be any number of galaxies too faint to be seen. The fainter ones are much redder than the brighter ones.

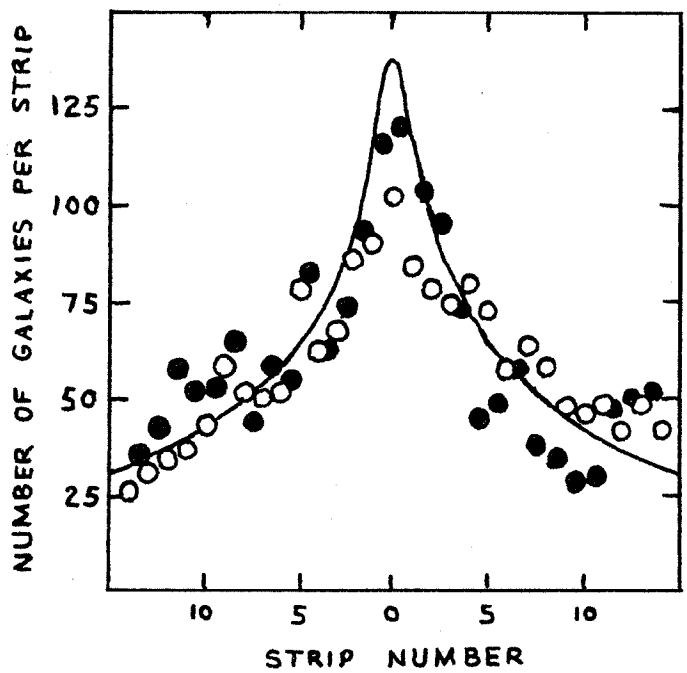

FIGURE 12. Abell's Counts. The circles are for south-north strips ordered east to west. The dots are for east-west strips ordered south to north.

The spatial distribution of the galaxies is independent of brightness. The velocities of the galaxies, due to the fewness of observations, appear to be consistent with both a circular-motion model and a radial-motion model. The observed root-mean-square velocity is 1050 km/sec.

PART II. PREVIOUS APPROACHES TO THE PROBLEM

ISOTHERMAL GAS SPHERE

Many scientists have concluded that the Coma cluster is in a steady state because the spatial distribution of its galaxies closely resembles the distribution of matter in an isothermal, spherically symmetric cloud of gas in static equilibrium in otherwise empty space. Such a cloud of gas is called an isothermal gas sphere (to be abbreviated IGS). The density in the IGS is given by

$$\rho(r) = \rho_0 \rho_1 \left(\frac{r}{\alpha}\right) \tag{2}$$

$$\alpha^2 = \frac{kT}{4\pi G \mu \rho_0} \tag{3}$$

where G = the Newtonian gravitational constant
k = the Boltzmann constant
μ = the molecular mass
T = the temperature
ρ_0 = the central density $\rho(0)$,

and $\rho_1(r_1)$ is the solution of the differential equation

$$\rho_1 = -\frac{1}{r_1^2} \frac{d}{dr_1} \frac{r_1^2}{\rho_1} \frac{d\rho_1}{dr_1} \tag{4}$$

with the boundary conditions $\rho_1(0) = 1$, $\left(\frac{d\rho_1}{dr_1}\right)_{r_1=0} = 0$.

Emden[15] has tabulated the numerical solution $\rho_1(r_1)$.

The actual solution $\rho_1(r_1)$ is asymptotic to $2/r_1^2$ around which it oscillates. The asymptotic function is the solution of the differential equation with $\rho_1(0) = \infty$. If the asymptotic solution is substituted into equation 2 and ρ_o is eliminated by means of equation 3, there results

$$\rho(r) = \frac{b}{r^2} \tag{5}$$

where

$$b = \frac{kT}{2\pi G\mu} . \tag{6}$$

(Equation 5 corresponds to model A_o.) The degree to which the physical configuration differs from this asymptotic configuration depends on how large α is. As α approaches zero, the actual solution $\rho(r)$ approaches the asymptotic solution of equations 5 and 6 —— the oscillations squeeze down on the asymptotic solution and squeeze in toward the origin. The point is that equations 5 and 6 can be used as a close approximation to an actual isothermal gas sphere.

The model with which to compare the Coma cluster has the density given by equation 2 within a sphere of radius R; the density is zero outside. Hubble[16] tabulated the projected density of an infinite IGS. From this density must be subtracted the projected

density of that part which lies beyond the radius $r_1 = R/\alpha$. The density to be subtracted is approximated by the asymptotic form obtained from equation 5. (This procedure is a little more accurate than Zwicky's method of subtracting a uniform density.) The projected-distribution function for the resulting projected density is shown in figure 13 for $\alpha = 0$, 1'.25, and 2'.

Zwicky took the radius of the cluster to be 160', so in order to compare his original work with the present analysis, his 18-inch counts (for his estimate of the density of field galaxies) are plotted as x's in figure 13 at radii contracted by the factor $\frac{100}{160}$. The dashed curve represents Zwicky's model of an IGS. The comparison of the dashed curve with the x's corresponds to Zwicky's original observation that the Coma cluster resembles an IGS.(17)

The dots and circles in figure 13 correspond to our interpretation of Zwicky's data, for which we use a radius of 100'. The IGS curves agree fairly well with the data. We conclude from figure 13 that the spatial distribution of galaxies in the Coma cluster closely resembles an IGS cut off at a radius of 100'.

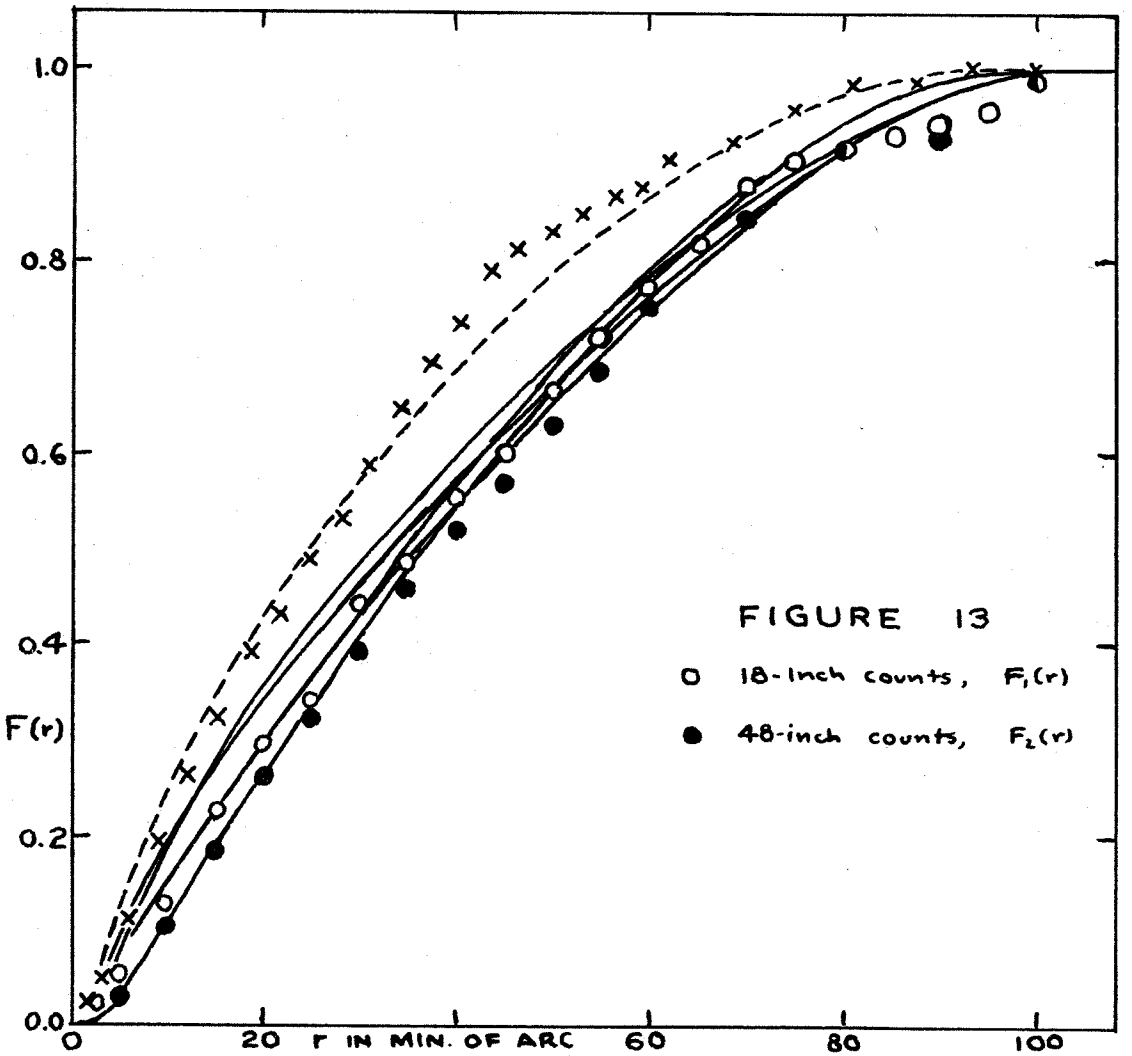

FIGURE 13

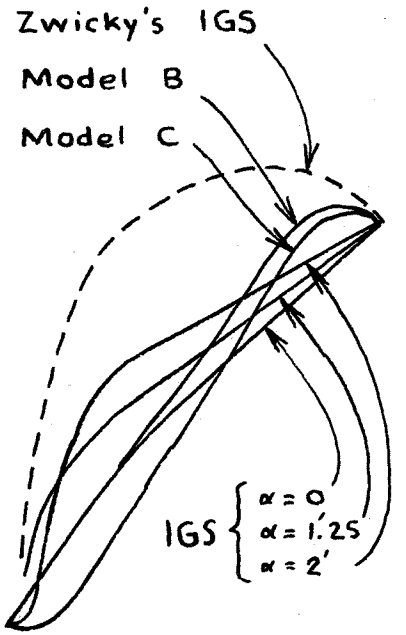

exaggerated curves for explanation

STRUCTURAL INDEX

Zwicky[18] has suggested a method for finding the mass of a cluster by determining the structural index α corresponding to its spatial distribution. For an IGS, the central projected density is given by

$$\zeta(0) = 6.06\,\alpha\rho_0 \ .$$

The temperature is assumed from kinetic theory to be given by

$$\overline{w^2} = \frac{3kT}{\mu} \ . \qquad (7)$$

Equation 3 becomes

$$\alpha^2 = \frac{\overline{w^2}}{12\pi G\rho_0} \ ,$$

where $\overline{w^2}$ is the mean square velocity of the galaxies. With $\overline{w^2}$ and α known and $\zeta(0)$ in galaxies per square degree, the mass per galaxy can be calculated.

It is doubtful whether a structural index α can be assigned to the Coma cluster for two reasons. (1) The closeness of the solution of equation 2 to equation 5 introduces some ambiguity into the method, as may be seen in figure 13. (2) What one considers to be counts of cluster galaxies depends on the estimate of the density of field galaxies. (Compare the x's and the circles in figure 13.)

There is also the difficulty raised by the possibility that the galaxies do not all have the same mass. An IGS composed of molecules of different masses is still an unsolved problem, as Zwicky pointed out.

There is a more reliable way to determine the mass of an IGS than by using the structural index. It involves the use of the virial theorem, to which we now proceed.

RELATIONSHIP BETWEEN THE ISOTHERMAL GAS SPHERE AND THE VIRIAL THEOREM

Both the virial theorem and the IGS differential equation will be derived in order to see the connection between them.

Consider a system of particles divided by a surface $\mathcal{S}$ into an interior region $\mathcal{R}$ and an exterior region. Let r_k^i be the i^{th} coordinate of the k^{th} particle's position, let w_k^i be the i^{th} component of its velocity, and let m_k be its mass. Define

$$\Psi = \sum_{\mathcal{R}} m_k r_k^i w_k^i$$

(repeated vector indices are summed). The summation extends over all particles in $\mathcal{R}$. Ψ can change in two ways: either the particles within $\mathcal{R}$ can

change their $r^i w^i$:

$$\frac{d}{dt}(m_k r_k^i w_k^i) = m_k w_k^i w_k^i + m_k r_k^i a_k^i ,$$

where $$a_k^i = \frac{dw_k^i}{dt} ;$$

or particles can pass through the surface $\mathcal{S}$, each carrying a contribution $-m_k r_k^i w_k^i$. The average rate of change of Ψ, averaged over a long time $\underline{t}$, is therefore given by

$$\overline{\frac{d\Psi}{dt}} = \overline{\sum_{\mathcal{R}} m_k w_k^i w_k^i} + \overline{\sum_{\mathcal{R}} m_k r_k^i a_k^i} - \iint_{\mathcal{S}} \bar{\sigma}\, r^i w^i w^j d^3w\, dS^j$$

where the bars refer to time averages, $\bar{\sigma}$ is the average density in phase space, d^3w refers to integration over velocity space, and dS^j refers to surface integration.

Assume that the system is in a steady state so that the average rate of change of Ψ is zero. Then

$$2\bar{T} + \overline{\sum_{\mathcal{R}} m_k r_k^i a_k^i} = \iint_{\mathcal{S}} \bar{\sigma}\, r^i w^i w^j d^3w\, dS^j \qquad (8)$$

where T is the kinetic energy $\sum_{\mathcal{R}} \frac{1}{2} m_k w_k^i w_k^i$.

If $\mathcal{R}$ were made to include the whole system so that the surface integral vanished, then we would have the usual form of the virial theorem

$$0 = 2\bar{T} + \overline{\Sigma\, m_k r_k^i a_k^i} .$$

For a gravitational system it follows that

$$0 = 2\overline{T} + \overline{V} \tag{9}$$

where $\underline{V}$ is the potential energy.

But now equation 8 will be applied to a stationary gas. For this case there is a continuous density ρ, and the velocities are isotropic. The surface integral becomes (app. III)

$$\int_S \tfrac{1}{3}\rho\overline{w^2}\, r^i dS^i ,$$

where $\overline{w^2}$ is the mean square velocity averaged over velocity space. Thus, equation 8 becomes

$$2T + \int_R \rho\, r^i a^i d\nu = \int_S \tfrac{1}{3}\rho\overline{w^2}\, r^i dS^i , \tag{10}$$

where $d\nu$ refers to volume integration. Application of Gauss' theorem results in

$$2T + \int_R \rho\, r^i a^i d\nu = \int_R r^i \nabla_i(\tfrac{1}{3}\rho\overline{w^2})d\nu + 2T$$

or $$\int_R r^i \left[\rho a^i - \nabla_i(\tfrac{1}{3}\rho\overline{w^2})\right] d\nu = 0 .$$

Because R and the origin for $\underline{r}^i$ are arbitrary,

$$\rho a^i = \nabla_i(\tfrac{1}{3}\rho\overline{w^2}) . \tag{11}$$

This is just the force law for a stationary gas with pressure $\frac{1}{3}\rho\overline{w^2}$ and field acceleration a^i. The IGS differential equation

$$\rho = -\frac{kT}{4\pi G\mu}\frac{1}{r^2}\frac{d}{dr}\frac{r^2}{\rho}\frac{d\rho}{dr}$$

(from which equations 2-4 are derived) is derived from equation 11 by (1) eliminating a^i by means of the field equation

$$4\pi G\rho = -\nabla_i a^i ,$$

(2) using equation 7, and (3) assuming spherical summetry.

The conclusion to be drawn from the foregoing is that the virial theorem and the IGS are alike in one respect but different in another respect. They are alike in that they deal with a system of particles in a steady state. The difference is that in the IGS the conditions are:

1. Isothermal —— the mean square velocity is independent of position.
2. Gas —— the velocities are isotropic; a spatial density exists.
3. Sphere —— there is spherical symmetry.

None of these conditions need be satisfied for the virial theorem.

The virial theorem in its usual form of equation 9 cannot be applied to an infinite IGS because its mass is infinite. In its generalized form, equation 8, the virial theorem applies but is the same as the IGS differential equation in integral form.

We can also conclude that applying the conventional virial theorem to a bounded IGS is the same as appealing to the structure of the IGS as Zwicky has done in using his structural index α. One advantage of using the virial theorem is that it eliminates the necessity of estimating either the central projected density or the structural index.

The mass of a bounded IGS obtained from equations 5 and 6 is 2/3 of the value that is obtained by applying the virial theorem. The reason for this is that no IGS is finite, and in order for the gas inside the boundary to resemble an IGS, there must be a wall to exert the pressure that would be exerted by the gas beyond the boundary. If the pressure of the wall is included in the virial theorem, then the calculated mass is reduced by the factor 2/3. To see this, we use model A_o for which the gravitational potential energy (to be derived later) is

$$V = -\frac{M^2}{RG}$$

where M is the total mass. The virial theorem gives

$$M\overline{w^2} = \frac{M^2}{GR} + 4\pi R^3 P \ ,$$

where P is the pressure exerted by the wall. This equation is of course the same as equation 10. The pressure P is taken to be χ times the pressure of the gas at $r = R$, i.e.,

$$P = \frac{\chi \overline{w^2}}{3} \frac{b}{R^2} = \frac{\chi M\overline{w^2}}{12\pi R^3} \ .$$

The mass is then given by

$$M = \frac{R\overline{w^2}}{G}\left(1 - \frac{\chi}{3}\right) \ .$$

On the one hand, if we require the wall to exert the pressure that would normally be exerted by the rest of the gas outside the boundary, then $\chi = 1$ and

$$M = \frac{2}{3} \frac{R\overline{w^2}}{G} \ .$$

Because of the relation between the virial theorem and the IGS presented above, this result is the same as that obtained by direct integration of equation 5 and substitution with equations 6 and 7:

$$M = 4\pi R b = \frac{2}{3} \frac{R\overline{w^2}}{G} \ .$$

On the other hand, if we reject the concept of a

wall, as will be done in this thesis, we have $\chi = 0$ and

$$M = \frac{R\overline{w^2}}{G} \ .$$

APPLICATION OF THE VIRIAL THEOREM

In applying the virial theorem to the Coma cluster, it is assumed (a) that the cluster is in a steady state, and (b) that the kinetic and potential energies at the epoch at which the cluster is observed are representative of the time averages of those quantities. Thus equation 9 is written in the form

$$2T + V = 0 \ . \tag{12}$$

Define M = the total mass of the cluster,

$\overline{w^2}$ = the mean square velocity, averaged over mass,

R = the radius of the cluster,

$\nu = -\frac{M^2}{GVR}$.

Then we may substitute

$$T = \frac{1}{2}M\overline{w^2}$$

and

$$V = -\frac{M^2}{GR\nu}$$

into equation 12. Solution for M gives

$$M = \frac{R\overline{w^2}}{G}\nu \ . \tag{13}$$

Equation 13 will be used to calculate the virial-theorem mass. The radius is 2.6 Mpc. Mayall's velocities are assumed to be representative of the velocities throughout the cluster.

$$\overline{w^2} = 3 \times (1050 \text{ km/sec})^2$$

or $$\overline{w^2} = 3.31 \times 10^6 \text{ km}^2/\text{sec}^2 .$$

(The factor 3 comes from the relation $\overline{w^2} = 3\overline{v^2}$.) It remains to determine ν.

The coefficient ν is determined by the spatial distribution of the mass in the cluster. For the case of spherical symmetry, there are two methods for calculating ν if the density $\rho(r)$ is known.

Method A. If $M^2(r)$ is the square of the mass inside a radius r, then

$$\nu = \frac{2M^2(R)}{R\int_0^\infty \frac{dr}{r^2} M^2(r)} . \qquad (14)$$

This is proved by substituting the field acceleration

$$g(r) = -\frac{M(r)}{Gr^2}$$

into the formula for potential energy:

$$-\frac{M^2}{GR\nu} = -\frac{1}{8\pi G}\int_0^\infty g^2 4\pi r^2 dr .$$

Method B.[19] (app. IV)

$$\nu = \frac{2}{R} \frac{\left(\int_0^\infty S \, dr\right)^2}{\int_0^\infty S^2 dr}$$

where $$S(r) = \int_r^\infty \rho(r') \, r' dr'$$

Method A will be used here.

In using the virial theorem it is assumed that the distribution of mass in the cluster is represented by the distribution of the galaxies. But instead of using the counts directly, it is simpler and as accurate to use a mathematical model approximating the observed counts. For model A, equation 14 gives

$$\nu = \frac{\left(1 - \frac{2}{3}\frac{c}{R}\right)^2}{1 - \frac{14}{15}\frac{c}{R} - \frac{2}{3}\frac{c}{R}\ln\frac{R}{c}} .$$

If c lies between 0 and 7.14 (fig. 9), then ν lies between 1.00 and 1.12. Schwarzschild,[19] in his treatment using method B and numerical integration, obtained

$$\nu = 0.89.$$

We adopt a value

$$\nu = 1.0 \pm 0.2 ,$$

which corresponds to model A_o.

The mass of the Coma cluster by the virial theorem is therefore

$$M = 2.0 \times 10^{15} M_{\odot} \qquad (15)$$

to an accuracy of 20 or 30 %. Following is a list of the assumptions used in deriving this figure.

1. The Coma cluster is in a steady state.

2. The kinetic and potential energies at the epoch at which the cluster is observed are representative of the time averages of these quantities.

3. Mayall's 40 velocities are representative of velocities throughout the cluster.

4. The cluster is spherically symmetric.

5. The spatial distribution of galaxies in the cluster is proportional to the spatial distribution of mass.

Another estimate of the mass is based on the assumption that the galaxies in the cluster are unable to escape from the cluster.* This gives only a minimum value for the mass. If r is the

---

* Sinclair Smith first used this approach in estimating the mass of the Virgo cluster.(20)

projected distance of a galaxy from the center of the cluster, and w is its velocity, then the mass can be no less than

$$\frac{rw^2}{2G} .$$

The maximum value for this quantity for any of the 40 galaxies whose velocities are known gives

$$M \geq 0.65 \times 10^{15} M_{\odot} .$$

This result involves less assumption than the virial theorem method, and it gives less information.

Schwarzschild's estimate of $3 \times 10^{14} M_{\odot}$ was based on a root-mean-square velocity deviation of 825 km/sec rather than 1050 km/sec, and he used a distance of 25Mpc instead of 90 Mpc.

THE MASS PROBLEM

We will now discuss the difficulty presented by the mass in equation 15. From the total photographic luminosity of the Coma cluster,

$$L = 4.3 \times 10^{12} L_{\odot} ,$$

results a mass-luminosity ratio of 470. Also, if there were only 1560 galaxies in the Coma cluster, then the average mass per galaxy would be $1.3 \times 10^{12} M_{\odot}$. Both of these values are much larger than for individual galaxies whose masses

have been calculated from velocity curves. Unfortunately, the latter include only spiral galaxies, whereas the Coma cluster is composed mainly of elliptical and SO galaxies. If the mass-luminosity ratio were the same for all galaxies in the Coma cluster, then the brighter galaxies would have huge masses —— 6.1×10^{13} $M_\odot$ for the brightest, 3.5×10^{13} $M_\odot$ for the second brightest, 1.7×10^{13} $M_\odot$ for the tenth brightest, and 0.56×10^{13} $M_\odot$ for the hundredth brightest.

For comparison figure 14 shows the galaxies whose masses have been calculated.[21] The coordinates are the logarithms of the mass and luminosity, so that a diagonal line represents a constant mass-luminosity ratio. The uncertainties, which are greater than the sizes of the circles would seem to indicate, are in some cases represented by lines. Also plotted are averages from Page's work on double galaxies. (The arrows indicate the more recent of his estimates.)

The mass-luminosity ratios fall within the range 0.2 to 80, and none of the galaxies have masses larger than 8×10^{11} $M_\odot$. The average Coma cluster galaxy falls outside these ranges. Even if there were three times as many galaxies in the Coma cluster so that the average mass were reasonable, the mass-luminosity ratio would still be just as

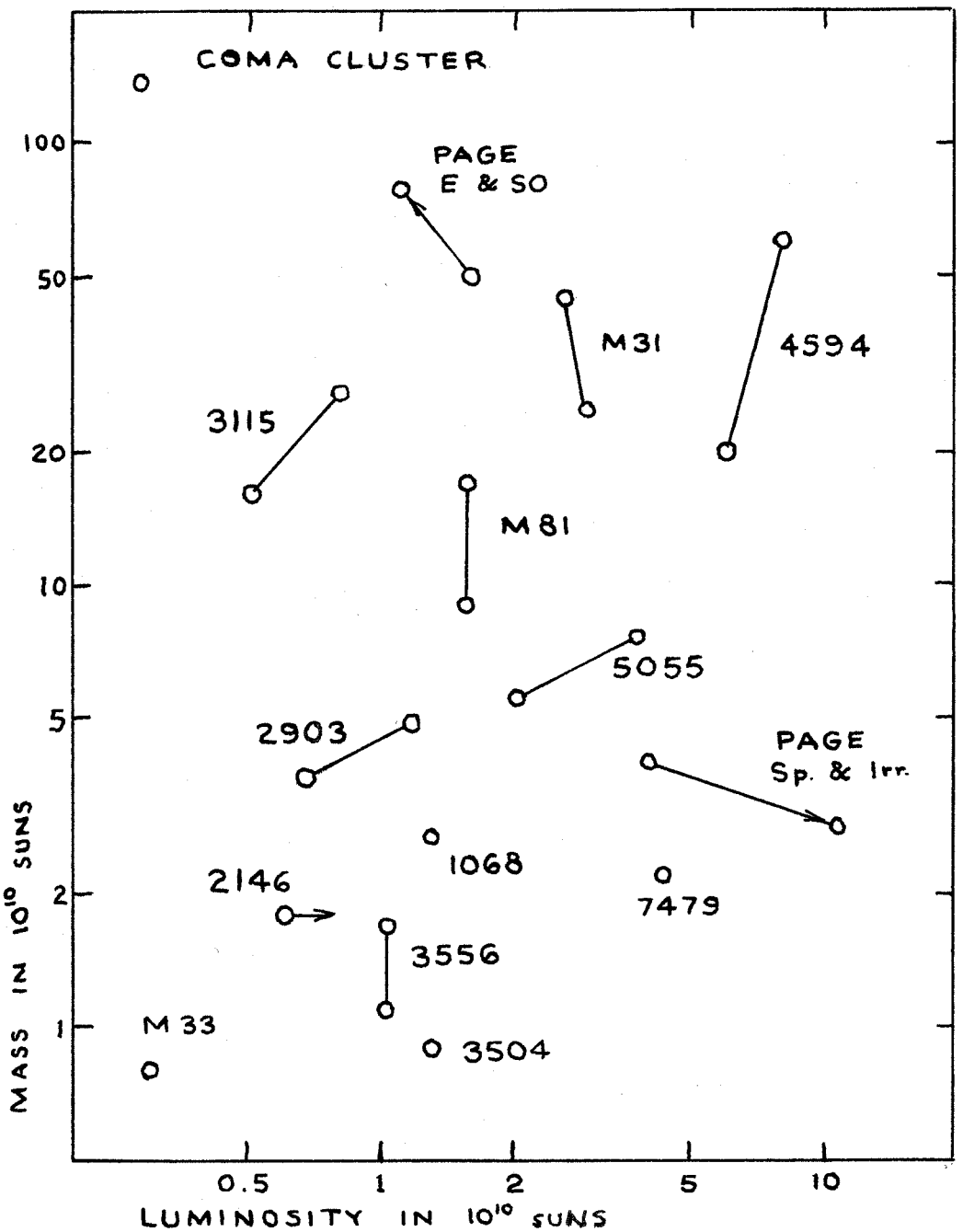
COMA CLUSTER
PAGE
E & SO
M31
4594
3115
M81
5055
2903
PAGE
Sp. & Irr.
1068
2146
7479
3556
M 33
3504
100
50
20
10
5
2
1
0.5
1
2
5
10
MASS IN 10^{10} SUNS
LUMINOSITY IN 10^{10} SUNS

FIGURE 14

high.

Resolution of the discrepancy is sought in two directions. On the one hand there could be intergalactic matter in the Coma cluster. Evidence seems to exclude the possibility that there is a mass anything like $2 \times 10^{15}\ M_{\odot}$ in the form of intergalactic neutral atomic hydrogen or intergalactic stars.(1)

On the other hand, if we try to force the mass down by a factor of, say, 20, then the potential energy of the cluster would equal one-tenth of the kinetic energy. Gravity would be negligible, and the cluster would be rapidly disrupting in a time the order of

$$\frac{2.6\ \text{Mpc}}{1050\ \frac{\text{km}}{\text{sec}}} = 2 \times 10^{9}\ \text{yr.}$$

However, it is argued that the spherical symmetry of the cluster and its resemblance to an isothermal gas sphere imply that it is in a steady state. This point will be examined more closely.

PART III. THE YOUNG-CLUSTER HYPOTHESIS

INTRODUCTION

Let us review the principal observational features of the Coma cluster which have thus far been presented.

1. The bright and faint galaxies have the same spatial distribution.
2. This distribution resembles that of an isothermal gas sphere cut off at a radius of about 100'.
3. There are many more faint galaxies than bright ones, and there may be any number of galaxies fainter than the plate limit.
4. The fainter galaxies are much redder than the brighter ones.

All four features are consistent with the hypothesis that the Coma cluster is a young cluster in which the galaxies are still evolving. (Feature 2 is usually thought to imply a steady state; however, there exist non-equilibrium configurations which resemble the IGS.) We now proceed to quantitatively compare the Coma cluster with a model representing a young cluster of galaxies.

The model to be used is as follows. In a spherical cloud of gas of uniform density

$$\rho_g = 3.6 \times 10^{-27} \text{ gm/cm}^3 \tag{16}$$

and radius $R = 2.6$ Mpc, galaxies begin forming at random times in random locations. The galaxies condense in a time the order of[22]

$$\left(\frac{3\pi}{32\, G\, \rho_g}\right)^{\frac{1}{2}} = 1.1 \times 10^9 \text{ yr} .$$

As a galaxy contracts, the pressure due to the gas becomes increasingly ineffective against the ever-decreasing area of the galaxy, so that the galaxy begins falling in the gravitational field of the cloud. The time to fall to the center of the cloud is the order of

$$\frac{\pi}{2\omega} = \left(\frac{3\pi}{16\, G\, \rho_g}\right)^{\frac{1}{2}} = 1.6 \times 10^9 \text{ yr} , \tag{17}$$

where ω^2 is the force constant. During its fall, the galaxy's contraction proceeds to the point where stars condense and then light up. The time for a star to contract gravitationally onto the main sequence is the order of 5×10^7 yr. The galaxy's continued journey through the original cloud will result in a flushing-out of interstellar gas, unless the cloud has been thinned out appreciably by galaxy

formation. Collisions with other galaxies, of which as many as 25 may occur in a single traversal of the cluster center, affect only the interstellar gas, and have little effect on the stars in the galaxies.[23] (App. V.) We are concerned only with the kinematics and the colors of the galaxies.

Two kinematical models will be used. In model B enough time has elapsed since the galaxies began forming that they are considered to be oscillating radially with random phases. In model C barely enough time has elapsed for the first-born galaxies to cross the cloud.

MODEL B

In model B it will be assumed that each galaxy moves in a potential

$$\phi(r) = \tfrac{1}{2}\omega^2 r^2$$

with a radial orbit of maximum radius α which we will call its amplitude. The orbits are distributed randomly in direction, and the galaxies in them are distributed randomly in phase. The fraction of galaxies having amplitudes between α and $\alpha+d\alpha$ is taken to be $3\alpha^2 d\alpha/R^3$ in order to agree with the uniform density of the original cloud.

The quarter-period of motion is

$$T = \frac{\pi}{2\omega} = \left(\frac{3\pi}{16\,G\rho_g}\right)^{\frac{1}{2}} = 1.57 \times 10^9 \text{ yr} .$$

The fraction of time that a galaxy of amplitude α spends within a spherical shell of radius r and thickness dr is

$$\frac{dr}{T\,w(\alpha,r)} ,$$

where $w(\alpha,r)$ is its velocity:

$$w(\alpha,r) = \omega\sqrt{\alpha^2-r^2} .$$

Because of the randomness of phase, this is equal to the fraction of galaxies of amplitude α that lie within the shell. Therefore, the fraction of galaxies with amplitudes between α and $\alpha+d\alpha$ that lies within the shell is

$$\frac{dr}{T\,w(\alpha,r)}\,\frac{3\alpha^2}{R^3}\,d\alpha . \qquad (18)$$

The density of galaxies is therefore given by

$$4\pi r^2\rho(r)\,dr = \int_{\alpha=r}^{R} \frac{dr}{T\,w(\alpha,r)}\,\frac{3\alpha^2}{R^3}\,d\alpha$$

or

$$\rho(r) = \frac{1}{4\pi r^2}\int_{\alpha=r}^{R} \frac{1}{T\,w(\alpha,r)}\,\frac{3\alpha^2}{R^3}\,d\alpha . \qquad (19)$$

The projected-distribution function corresponding to this density is (app. IC)

$$F(r) = \frac{1}{2}\frac{r}{R}\left(3-\frac{r^2}{R^2}\right). \qquad (20)$$

(Fig. 13.) This model agrees well with the observed counts.

The ratio $\sqrt{\Upsilon}$ of the maximum velocity to the root-mean-square velocity can be derived without difficulty. The mean square velocity of galaxies of amplitude α is $\frac{1}{2}\omega^2\alpha^2$. Therefore the mean square velocity for all the galaxies is

$$\overline{w^2} = \int_0^R \frac{1}{2}\omega^2\alpha^2\,\frac{3\alpha^2}{R^3}\,d\alpha = \frac{3}{10}\omega^2R^2.$$

The maximum velocity is $w_{max} = \omega R$. Therefore

$$\Upsilon = \frac{w_{max}^2}{\overline{w^2}} = \frac{10}{3} = 3.3 \ .$$

The observed ratio is

$$\Upsilon = \frac{(2500)^2}{3\ (1050)^2} = 1.9 \ .$$

To resolve the discrepancy we should observe galaxies with velocities as high as 3300 km/sec.

Because of this discrepancy, the mass calculated with the model will depend on whether the observed rms velocity $1050\sqrt{3}$ km/sec or the observed maximum velocity 2500 km/sec is used. The density and quarter-period chosen for the model in equations 16 and 17 correspond to the latter. The total mass

is then

$$M = 4.0 \times 10^{15}\ M_{\odot}\ . \qquad (21)$$

On the other hand, if $w_{max} = 3300$ km/sec, then

$$M = \frac{3.3}{1.9} \times 4.0 \times 10^{15}\ M_{\odot} = 7.0 \times 10^{15}\ M_{\odot}\ . \qquad (22)$$

The value for the mass given in equation 21 is chosen for use in the model because it lies between the extremes of equations 15 and 22.

The difference between the values given in equations 15 and 22 seems at first sight like a contradiction, because the virial theorem applies to model B; the kinematics of model B refer to a steady state. The difference lies in the fact that although the objects in model B have a spatial density approximating model A_o, the mass density in model B is uniform. It should be emphasized that model B predicts the distribution of the galaxies themselves without reference to their masses.

Model B has been compared with observation in two respects: (1) the distribution in v-r space, and (2) the spatial distribution. The first shows no inconsistency because the observations are not numerous enough, and the second shows good agreement. The density of galaxies in model B is proportional to

$$\frac{\varphi_{\frac{1}{2}}\left(\frac{r^2}{R^2}\right)}{r^2} .$$

The function $\varphi_{\frac{1}{2}}(x)$, to be discussed later, does not vary greatly over a wide range in x (fig. 15). It is this property of having the density be nearly proportional to r^{-2} which makes model B so similar to model A_o. It is of interest to see that there are variations of model B which have the same property.

VARIATIONS OF MODEL B

Model B can be generalized to include other forms of the potential $\phi(r)$. We will also generalize the distribution in amplitude by replacing $3\alpha^2 d\alpha/R^3$ with $f(\alpha)d\alpha$. The previous analysis follows through up to equation 19, except that now we have

$$\rho(r) = \frac{1}{4\pi r^2} \int_r^R \frac{1}{T(\alpha)w(\alpha,r)} f(\alpha)d\alpha \qquad (23)$$

where $$w(\alpha,r) = \sqrt{2}\sqrt{\phi(\alpha) - \phi(r)}$$

and $$T(\alpha) = \int_{r=0}^{\alpha} \frac{dr}{w(\alpha,r)} .$$

In order to have the integrand be a function of

only one argument,

$$u = \frac{\sqrt{\phi(\alpha) - \phi(r)}}{\sqrt{\phi(R)}}$$

is used as the variable of integration instead of α. Then equation 23 becomes

$$\rho(r) = \frac{1}{r^2} \int_0^{\sqrt{1 - \frac{\phi(r)}{\phi(R)}}} Q\left[u^2 + \frac{\phi(r)}{\phi(R)}\right] du$$

where $$Q\left[\frac{\phi(\alpha)}{\phi(\alpha)}\right] = \frac{\sqrt{\phi(R)}\ f(\alpha)}{2\sqrt{2}\pi T(\alpha) g(\alpha)}$$

and $g(\alpha)$ is the magnitude of the gravitational acceleration, $\left|\frac{d\phi}{d\alpha}\right|$. We will now prove that there exist various forms for $Q(x)$ for which $r^2\rho(r)$ is nearly constant over a wide range in $\underline{r}$.

In general $\phi(r)$ and $f(r)$ can be expanded in power series

$$\phi(r) = r^n \sum_{k=0}^{\infty} a_k r^k \qquad f(r) = r^m \sum_{k=0}^{\infty} b_k r^k$$

so that $Q(x)$ can be expressed as a power series

$$Q(x) = x^q \sum_{k=0}^{\infty} c_{k+q} x^k$$

where $$q = \frac{m}{n} - \frac{1}{2} .$$

If we define

$$\varphi_q(x) = (2q+1)\int_0^{\sqrt{1-x}} (u^2+x)^q du ,$$

then $$r^2\rho(r) = \sum_{k=q}^{\infty} \frac{c_k}{2k+1} \varphi_k\left[\frac{\phi(r)}{\phi(R)}\right] .$$

If $\phi(r)$ and $f(r)$ are pure powers of r, then only one $\varphi_k(x)$ will appear. In general there will be an expansion involving all of them.

Some of the functions $\varphi_q(x)$ are shown in figure 15.* The property of special interest to us is that, for a wide range in q, the functions do not differ from unity to a significant extent until their plunge to zero at $x=1$. For example, for $q \leq 2\frac{1}{2}$, the functions do not differ from unity by more than a factor of two over a wide range of x. It is clear that there are combinations of the form

$$\frac{\sum_{k=q}^{\infty} \frac{c_k}{2k+1} \varphi_k(x)}{\sum_{k=q}^{\infty} \frac{c_k}{2k+1}}$$

which have the same property.

---

* From the identity

$$\int (u^2+x)^q du = \frac{u}{2q+1} (u^2+x)^q + \frac{2qx}{2q+1} \int (u^2+x)^{q-1} du$$

is derived an iteration formula,

$$\varphi_q(x) = \sqrt{1-x} + \frac{2q}{2q-1} x \varphi_{q-1}(x) ,$$

useful in deducing mathematical properties of the functions and in computing their numerical values.

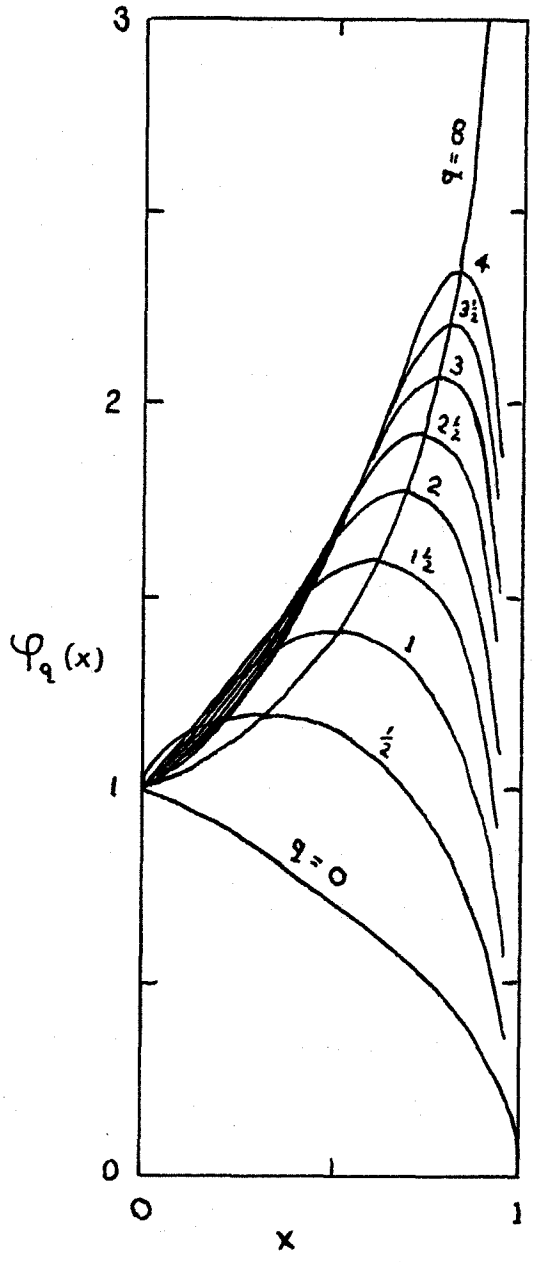

FIGURE 15

The projected-distribution functions for

$$\rho(r) \propto \frac{\varphi_\infty\left(\frac{r^2}{R^2}\right)}{r^2}$$

and

$$\rho(r) \propto \frac{\varphi_o\left(\frac{r^2}{R^2}\right)}{r^2}$$

are shown in figure 16. The latter has a projected density proportional to

$$\frac{1}{r} - \frac{1}{R}$$

which resembles Zwicky's approximation to a finite IGS; $\frac{1}{r}$ is the projected density of the asymptotic form of an IGS, and $\frac{1}{R}$ is the constant subtracted density.

MODEL C

In model C it is assumed that K galaxies are formed per unit volume per unit time in the original cloud. For simplicity K is treated as a constant. The number of galaxies found in a spherical shell of radius r and thickness dr which fell from a radius α is

$$K4\pi\alpha^2 d\alpha \frac{dr}{w(\alpha,r)} , \qquad (24)$$

where $w(\alpha,r)$ is the velocity:

$$w(\alpha,r) = \omega\sqrt{\alpha^2-r^2} .$$

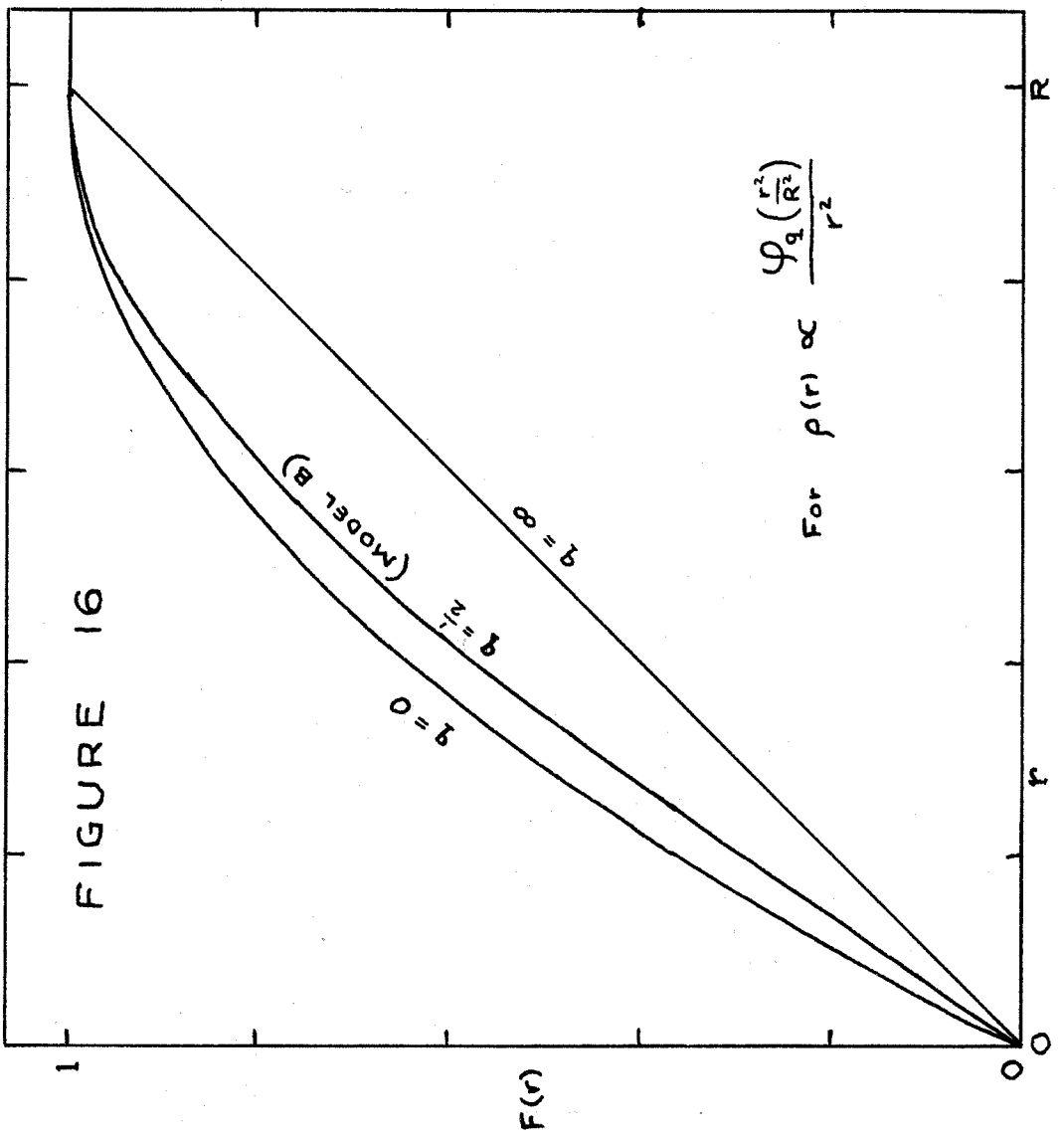
FIGURE 16
For $\rho(r) \propto \frac{\varphi_q\left(\frac{r^2}{R^2}\right)}{r^2}$
$q = \infty$
$q = \frac{1}{2}$
(MODEL B)
$q = 0$
F(r)
1
0
0
r
R

To find the density $\rho(r)$ of galaxies at a radius r, expression 24 is integrated over all α. Two cases occur: either $r > R\cos\omega t$ or $r < R\cos\omega t$. If $r > R\cos\omega t$, then

$$4\pi r^2\rho(r)\,dr = \int_{\alpha=r}^{R} K4\pi\alpha^2 d\alpha \frac{dr}{w(\alpha,r)} . \qquad (25)$$

If $r < R\cos\omega t$, then

$$4\pi r^2\rho(r)\,dr = \int_{\alpha=r}^{\frac{r}{\cos\omega t}} K4\pi\alpha^2 d\alpha \frac{dr}{w(\alpha,r)} .$$

When the integrations are carried out, it is found that the density $\rho(r)$ for $r < R\cos\omega t$ is a constant equal to $\rho(R\cos\omega t)$ from equation 25. This is due to the fact that the density of a uniform sphere remains uniform under free gravitational contraction.

A comparison of expressions 18 and 24 shows that model C is the same as model B in the region $r > R\cos\omega t$, except for a normalization factor. For normalization we set

$$\frac{4}{3}\pi R^3 Kt = 1.$$

Then the ratio of expression 24 to expression 18 is T/t or $\pi/2\omega t$. Indeed, when $\omega t = \pi/2$, model C is identical with model B.

Consider the case $\omega t < \pi/2$. For $r > R\cos\omega t$,

the distribution of galaxies in model C is the same as in model B except multiplied by the ratio $\pi/2\omega t$. Therefore, from equation 20 we get for model C:

$$1 - F(r) = \frac{\pi}{2\omega t}\left[1 - \frac{1}{2}\frac{r}{R}\left(3 - \frac{r^2}{R^2}\right)\right] .$$

The use of model C with the shorter time scale allows us to pull the $F(r)$ curve in figure 13 down to more nearly agree with the 48-inch counts at small r. The curve for model C in figure 13 corresponds to $\pi/2\omega t = 1.05$. The curve for model B is the same as for model C with $\pi/2\omega t = 1.00$.

The difference in t,

$$t = \frac{\pi}{2\omega}\left(\frac{1}{1.00} - \frac{1}{1.05}\right) = 7.5 \times 10^7 \text{ yr}$$

might possibly represent the difference between the ages of the brighter 18-inch galaxies and the fainter 48-inch galaxies. This value is the same order of magnitude as the time for stars to light up.

In order to have model C agree with the observations, the galaxies must have a uniform probability to light up at any time during the interval t. If the galaxies lit up only at a time t, then they would all be concentrated within a sphere of radius $R \cos \omega t$.

This study can hardly be considered conclusive. The purpose is only to show the possibility of using non-equilibrium kinematics for a cluster of galaxies.

THE L'-L DIAGRAM

The path taken by an evolving galaxy on the L'-L diagram will be predicted theoretically, and then it will be compared with the distribution of Coma cluster galaxies.

It is convenient to use the horizontal displacement D of a galaxy from the line

$$L' = L \cdot 10^{-0.4\ I_o},$$

where I_o is the color index of the galaxy when it is mature (fig. 17). D is defined

$$D = L - L' \cdot 10^{0.4\ I_o}.$$

If L_1 and L_1' are the photovisual and photographic luminosities of the stars that are still in the process of formation, then $L - L_1$ and $L' - L_1'$ are the photovisual and photographic luminosities of the mature stars in the galaxy. Therefore

$$\frac{L - L_1}{L' - L_1'} = 10^{0.4\ I_o}.$$

It follows that

$$D = L_1 - L_1' \cdot 10^{0.4\ I_o}. \qquad (26)$$

In Jeans' concept of galaxy evolution, a portion of gas first contracts to form a galaxy, and then portions of the material in the galaxy condense

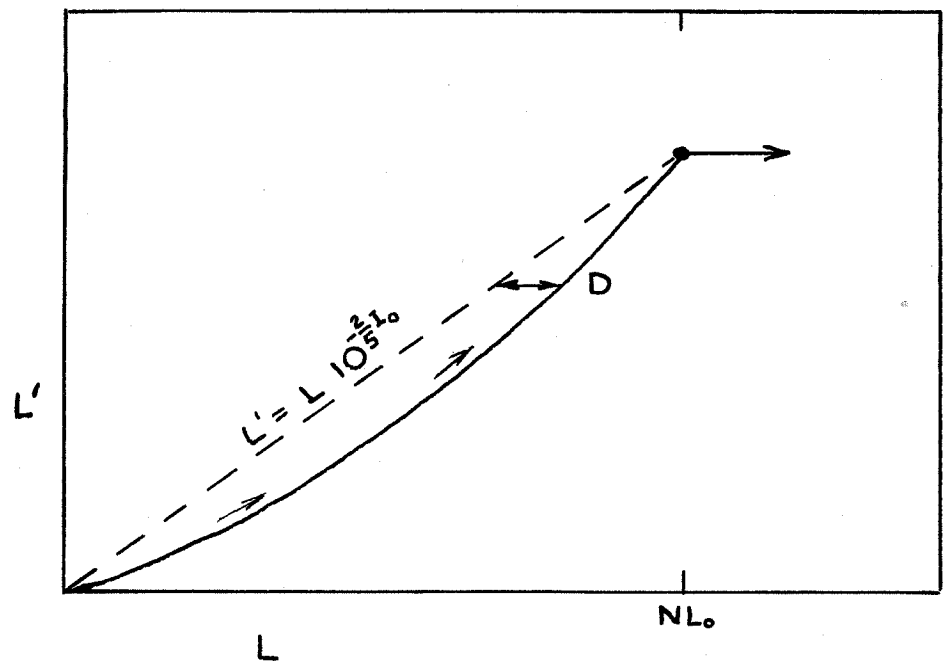

FIGURE 17

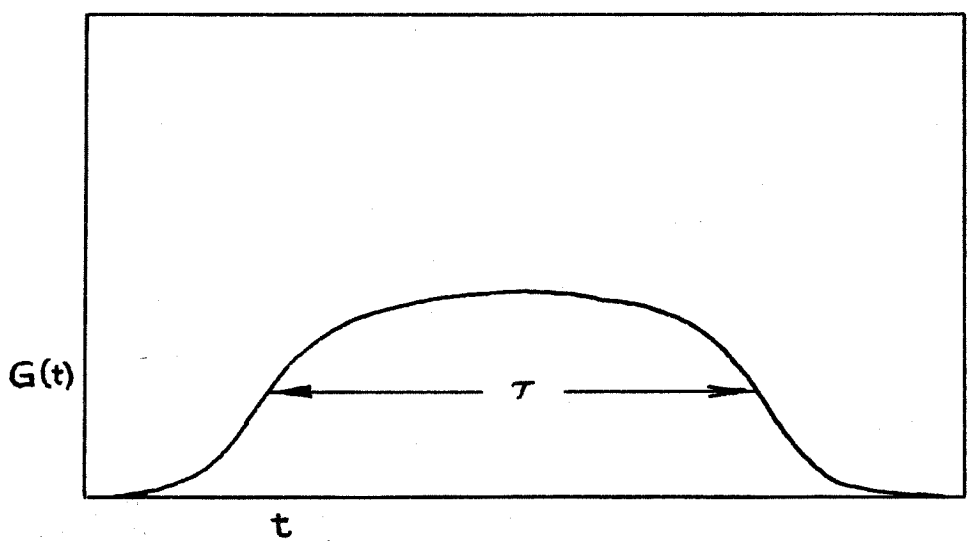

FIGURE 18

into stars.[22] We assume that the stars are all of the same type, and that they are born at a rate $G(t)$ as shown qualitatively in figure 18. Let τ represent the width of the curve. After each star is born, it evolves in accordance with the usual theory of gravitational contraction.[24] The star's bolometric luminosity L_b, temperature θ, and radius R are related by the equations

$$L_b \propto R^{-n}$$

$$\frac{dR}{dt} \propto L_b R^2$$

$$L_b \propto R^2 \theta^2$$

where n is a parameter which lies between 0.5 and 0.78. If these equations are solved for L_b and θ as functions of time $t = \xi t_o$, then

$$L_b = L_{b_o} \xi^{n/1-n} \tag{27}$$

and

$$\theta = \theta_o \xi^{(2+n)/4(1-n)}, \tag{28}$$

where ξ is the fraction of time that the star has been evolving. (The subscript o refers to the final state of the star.) The total time t_o is the order of 5×10^7 years.

The color index I (0.68 larger than the conventional definition) is assumed to be given by

$$I = \frac{7200^\circ K}{\theta} , \tag{29}$$

and the bolometric correction $\beta(I)$ is assumed to be the same function of color index as for main sequence stars.[13] The photovisual and photographic luminosities of the star are given by

$$L = L_b \, 10^{0.4\beta}, \tag{30}$$

$$L' = L_b \, 10^{0.4\,(\beta - I)}, \tag{31}$$

respectively. The color index can be expressed as a function of ξ by means of equations 28 and 29:

$$I = I_o \, \xi^{-(2+n)/4(1-n)} . \tag{32}$$

The substitution of equations 27, 30, and 31 into equation 26 and integration over $G(\xi t_o) t_o d\xi$ gives

$$D = \int_o^1 G(\xi t_o) L_o \, \xi^{\frac{n}{1-n}} \, 10^{\frac{2}{5}\left\{\beta[I(\xi)] - \beta_o\right\}} \left\{1 - 10^{\frac{2}{5}[I_o - I(\xi)]}\right\} t_o \, d\xi .$$

The integration is simplified by using I as the variable of integration by means of equation 32.

$$D = \frac{4(1-n)}{2+n} \, I_o^{\frac{4}{2+n}} \, L_o t_o \int_{I_o}^{\infty} G[t_o \xi(I)] \, J(I) \, dI$$

where

TABLE 5. J(I)

I	$-\beta$	J
1.0	0.00	0.000
1.1	0.02	0.068
1.2	0.05	0.102
1.3	0.09	0.115
1.4	0.10	0.121
1.5	0.16	0.116
1.6	0.36	0.094
1.7	0.57	0.074
1.8	0.75	0.060
1.9	0.94	0.048
2.0	1.15	0.037
2.1	1.35	0.029
2.2	1.75	0.019
2.3	2.30	0.010
2.4	2.85	0.006
2.5	3.3	0.004
2.6	3.8	0.002

The bolometric correction is extrapolated to I larger than 2.1 by use of the red giants.

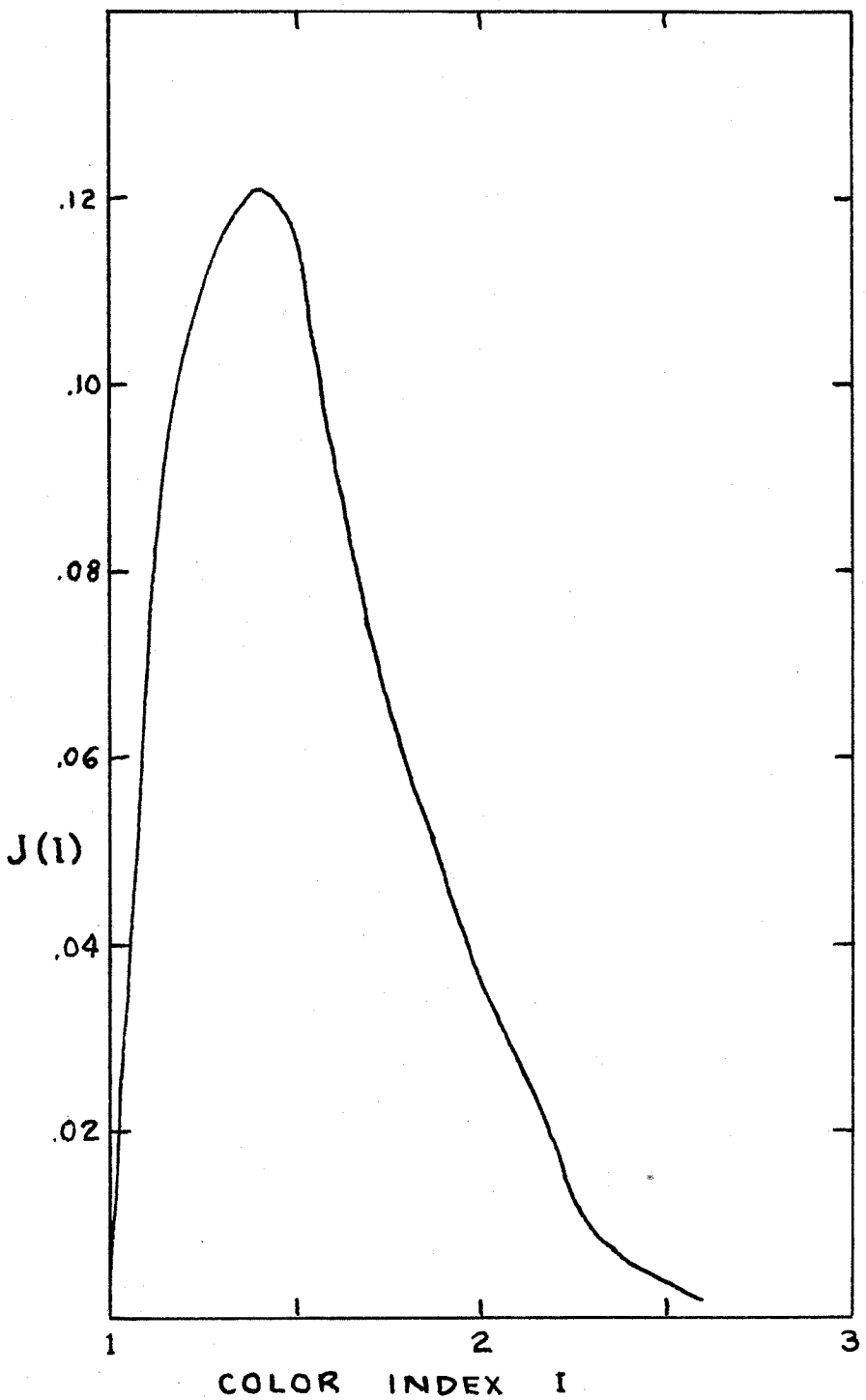

FIGURE 19

$$J(I) = 10^{0.4[\beta(I) - \beta_o]} I^{-\frac{6+n}{2+n}} \left[1 - 10^{-0.4(I-I_o)}\right]. \qquad (33)$$

The power $-\frac{6+n}{2+n}$ to which I is raised in equation 33 is not sensitive to n; the power is taken to be -2.5. I_o is taken to be unity.

The function $J(I)$ is shown in figure 19 where it is seen to have a rapid cut-off at large I. Because of this cut-off, D is most sensitive to the value of $G(t)$ near $I = 1$, i.e., near $t = t_o$. If $G(t)$ were a constant equal to N/τ, then

$$D = \frac{4(1-n)}{2+n}\, 0.09\, \frac{NL_o t_o}{\tau} . \qquad (34)$$

If $G(t)$ is of the form shown in figure 18, then as time goes on, D will first rise to a maximum value given approximately by equation 34, and then it will fall to zero. At the same time, the luminosity will rise from zero and increase to full brilliance at $L = NL_o$. Thus, during its evolution, the galaxy will trace out a track in the L'-L diagram such as the one shown in figure 17. After it has reached the point of maturity, a galaxy will begin moving to the right as its brighter stars evolve into red giants.

There is approximate agreement between figures 11 and 17. We conclude that there is no inconsistency between the colors of the galaxies and the

hypothesis that they are still evolving. The average point of maturity in figure 11 might be at $L = 2 \times 10^{-6} = NL_o$, and $\underline{D}$ is the order of 1×10^{-7}. Equation 34 then gives

$$\frac{\tau}{t_o} = \text{the order of unity,}$$

which says that the time τ for most of the stars to be born is the same order of magnitude as the time t_o for a star to evolve onto the main sequence, namely 5×10^7 years.

THE MASS PROBLEM

We now return to the problem of the large mass of the Coma cluster. During its evolution, a galaxy will move along a line of constant mass in figure 14 until it reaches full luminosity. Let the diagonal line in figure 20 represent the mass-luminosity ratio of the average galaxy at full brightness. Under the hypothesis that the galaxies in the Coma cluster are still evolving, each will be to the left of the diagonal line, moving horizontally toward it. The points in figure 20 represent one possibility. Only the horizontal distribution of the points can be observed. One could wish to observe the vertical distribution in order to settle the mass problem, but we must be content with guessing. The average mass for the points shown in figure 20 is the order

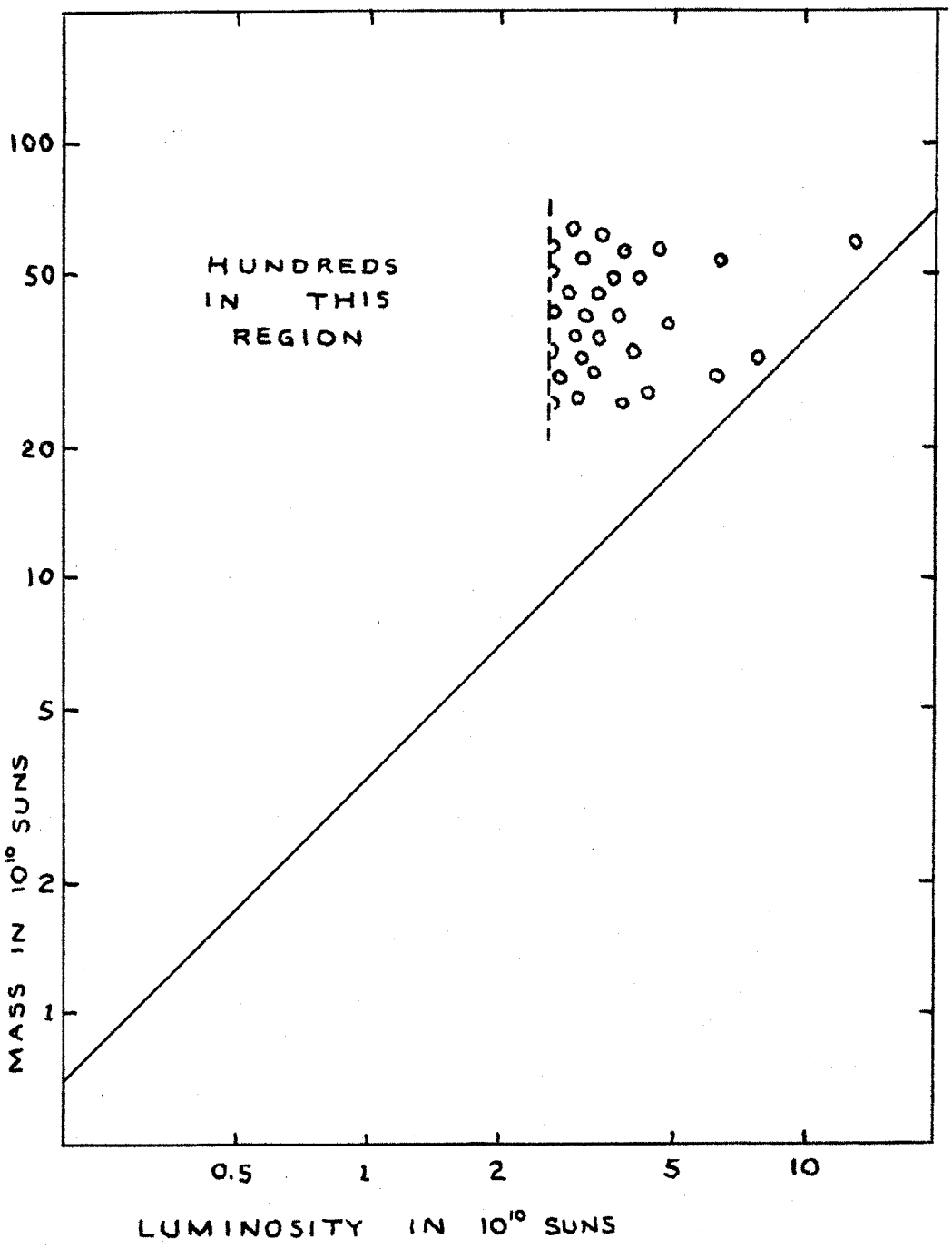
HUNDREDS
IN THIS
REGION
100
50
20
10
5
2
1
MASS IN 10^{10} SUNS
0.5
1
2
5
10
LUMINOSITY IN 10^{10} SUNS

FIGURE 20

of 3×10^{11} $M_\odot$, and the total number of galaxies is around 13,000.

In the hypothesis of evolving galaxies, the solution to the mass problem is that the unseen mass is largely in the form of young galaxies too faint to be seen and uncondensed matter in the faint galaxies that are seen. Such unseen matter would be difficult to detect because of the smaller area presented to us. For example, 13,000 spheres of 10 kpc radius, all in plain view, would present an area only 20% of the area of the whole cluster.

CONCLUSION

The observational features of the Coma cluster are not inconsistent with a hypothesis that it is a young cluster. The distribution of matter in an isothermal gas sphere is not so unique as to allow conclusions to be drawn from any resemblance between it and an actual system. The model suggested in this investigation has an age of around 2×10^9 years, many times smaller than Zwicky's estimate of 10^{18} years and well within the time scale of the exploding models of the universe.(25)

of 3×10^{11} $M_{\odot}$, and the total number of galaxies is around 13,000.

In the hypothesis of evolving galaxies, the solution to the mass problem is that the unseen mass is largely in the form of young galaxies too faint to be seen and uncondensed matter in the faint galaxies that are seen. Such unseen matter would be difficult to detect because of the smaller area presented to us. For example, 13,000 spheres of 10 kpc radius, all in plain view, would present an area only 20% of the area of the whole cluster.

CONCLUSION

The observational features of the Coma cluster are not inconsistent with a hypothesis that it is a young cluster. The distribution of matter in an isothermal gas sphere is not so unique as to allow conclusions to be drawn from any resemblance between it and an actual system. The model suggested in this investigation has an age of around 2×10^{9} years, many times smaller than Zwicky's estimate of 10^{18} years and well within the time scale of the exploding models of the universe.(25)

REFERENCES

1. Burbidge and Burbidge, Ap. J. 130, 629 (1959). Vaucouleurs, Ap. J. 131, 585 (1960).

2. Hubble and Humason, Ap. J. 74, 43 (1931). Shapley, Harvard Bulletin 896 (1934). Zwicky, Morphological Astronomy (1957), p. 68. Zwicky, Handbuch der Physik, v. 53 (1959).

3. Zwicky, Morphological Astronomy (1957), pp. 123-125.

4. Sandage, Ap. J. 127, 513 (1958).

5. Hubble, Ap. J. 79, 8 (1934); Realm of the Nebulae (1936), pp. 184-189.

6. Zwicky, Ap. J. 86, 217 (1937), pp. 241-245.

7. Zwicky, Morphological Astronomy (1957), pp. 37-50. In Table II on page 41 there is an error due to adding both of the first two lines. The total number of galaxies should be 804.

8. Zwicky, Pub. A.S.P. 63, 61 (1951) and 64, 247 (1952).

9. Shane and Wirtanen, An. J. 64, 197 (1959), figure 4.

10. Abell, in preparation.

11. Stebbins, Whitford, and Johnson, Ap. J. 112, 469 (1950).

12. Shane and Wirtanen, An. J. 59, 285 (1954), p. 297.

13. Payne-Gaposchkin, Introduction to Astronomy (1954), pp. 279, 280. Other authors use 0.68 instead of 0.64 in the color index formula.

14. Pettit, Ap. J. 120, 413 (1954).

15. Emden, Gaskugeln, Anwendungen der Mechanischen Wärmetheorie (1907), Neuntes Kapitel, pp. 131-148.

16. Hubble, Ap. J. 71, 274 (1930), table XIII.

17. Zwicky, Pub. A.S.P. 54, 185 (1942); Ap. J. 95, 555 (1942).

18. Zwicky, Ap. J. 95, 555 (1942); Morphological Astronomy (1957), pp. 136-143; Handbuch der Physik, v. 53 (1959), p. 401.

19. Schwarzschild, An. J. 59, 273 (1954).

20. Sinclair Smith, Ap. J. 83, 23 (1936).

21. Burbidge, Burbidge, and Prendergast, Ap. J.

NGC 1068	130	26
NGC 2146	130	739
NGC 5055	131	282
NGC 3556	131	549
NGC 2903	132	640
NGC 7479	132	654 *
NGC 3504	132	661

Burbidge and Burbidge, Ap. J. 130, 17 (1959) and 130, 629 (1959), pp. 634 ff.
Münch, An. J. 62, 28 (1957) for M81.
Page, An. J. 64, 53 (1959) and Ap. J. 132, 911 (1960) for double galaxies.
Schmidt, B.A.N. 14, 17 (1957) for M31.
Schwarzschild, An. J. 59, 273 (1954).

22. Jeans, Astronomy and Cosmogony (1929), pp. 345-357 of chapter XIII.

23. Spitzer and Baade, Ap. J. 113, 413 (1951)

24. Burbidge and Burbidge, Handbuch der Physik, v. 51 (1958), pp. 157-160.
Schwarzschild, Structure and Evolution of the Stars (1958), pp. 156-164.

25. Zwicky, Proc. Nat. Acad. 25, 604 (1939).
Zwicky, Pub. A.S.P. 72, 365 (1960).

26. Humason, Mayall, and Sandage, An. J. 61, 97 (1956), p. 155.

* The luminosity of NGC 7479 was computed from its apparent magnitude.(26)

APPENDIX

I. v-r Distribution.

   A. Explosion.

   B. Circular Orbits.

   C. Model B.

II. Abell's Plate Fraction f.

III. The Surface Integral $\iint \bar{\sigma}\, r^i w^i w^j d^3w\, dS^j$ for a Gas.

IV. Method B.

V. Collisions.

APPENDIX I. v-r DISTRIBUTION

A. EXPLOSION

Model A_o is used for the density of objects in the exploding model. Each object has a velocity

$$\vec{w} = \frac{\vec{r}}{T} ,$$

where $\vec{r}$ is its distance from the center and T is the time since the beginning of the explosion. With reference to figure 21, it is seen that

$$\sigma(r,v)\,dr\,dv = 2\pi r\,dr\,\rho\,dx ,$$

where $v = \frac{x}{T}$, $\rho = \frac{b}{r^2+x^2}$, and $\sigma(r,v)$ is the density in v-r space. There results

$$\sigma(r,v) = \frac{2\pi T b r}{r^2 + T^2 v^2} ,$$

provided $(r^2 + T^2v^2) < R^2$. The density $\sigma(r,v)$ is shown in figure 2.

B. CIRCULAR ORBITS

In the circular-orbit model each galaxy moves in a circular orbit under the influence of a gravitational field caused by a density of matter of the form given by model A_o. All galaxies have the same velocity

$$w_o = \sqrt{4\pi G b} .$$

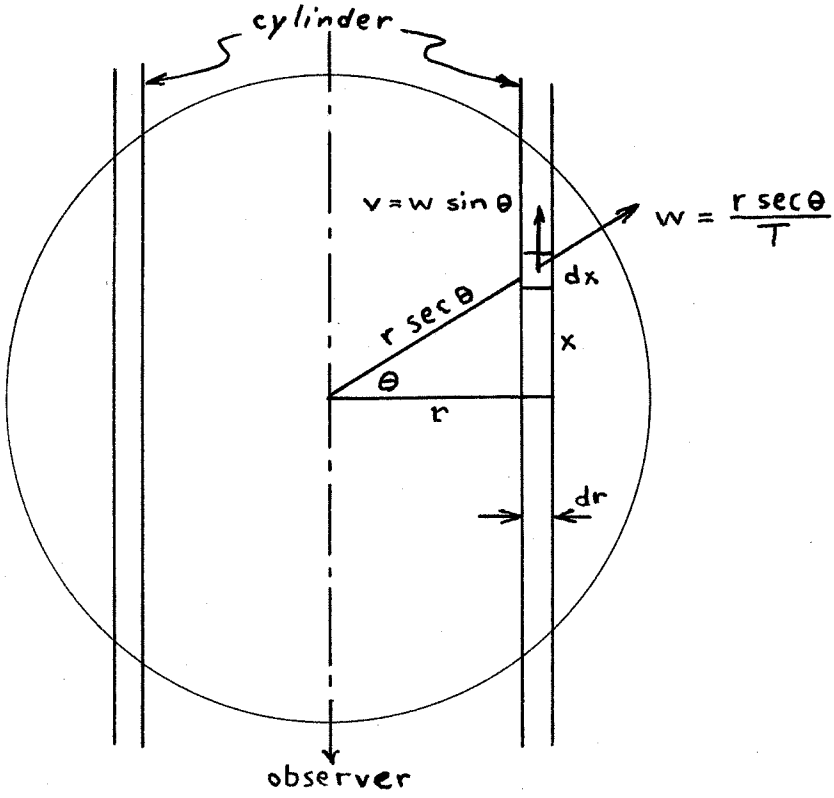

FIGURE 21

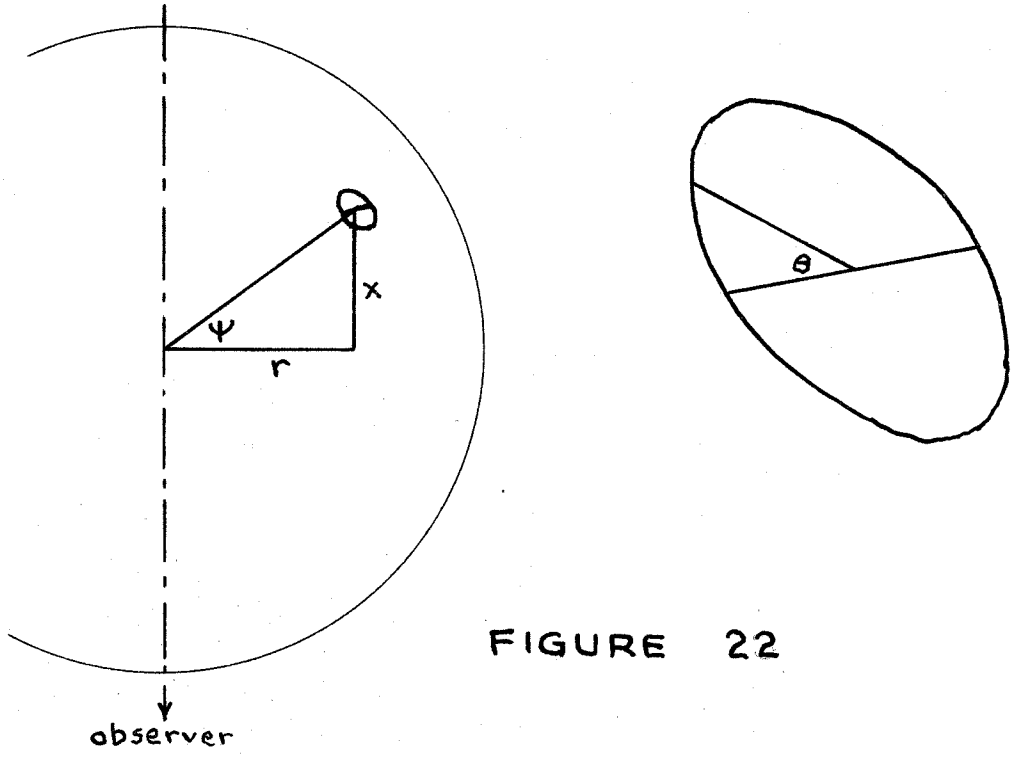

FIGURE 22

The orbits are distributed at random so that at any point $\underline{r},\underline{x}$ (fig. 22) the fraction of galaxies having line-of-sight velocities between v and $v+dv$ is equal to $d\theta/\pi$, where θ is given by

$$\sin\theta = \frac{v \sec\Psi}{w_o} \tag{35}$$

and

$$\Psi = \tan^{-1}\frac{x}{r} . \tag{36}$$

The density of galaxies is assumed also to be given by model A_o:

$$\rho(r) = \frac{1}{4\pi R(r^2+x^2)} .$$

Therefore, the density in $\underline{v}$-$\underline{r}$ space is given by

$$\sigma(r,v) = 2\cdot 2\pi r \int_{x=0}^{\sqrt{R^2-r^2}} \frac{d\theta}{\pi dv} \frac{dx}{4\pi R(r^2+x^2)} .$$

Substitution with equations 35 and 36 yields

$$\sigma(r,v) = \frac{1}{\pi R} \int_0^{\Psi_o} \frac{d\Psi}{\sqrt{w_o^2\cos^2\Psi - v^2}} .$$

The cosine of the upper limit Ψ_o is either $\frac{r}{R}$ or $\frac{v}{w_o}$, whichever is larger. Substitution with $v = w_o\cos\alpha$ and $\sin\Psi = \sin\alpha\sin\varphi$ results in an elliptic integral of the first kind:

$$\sigma(r,v) = \frac{1}{\pi R w_o} F(\alpha,\varphi) ,$$

where $\varphi = \frac{\pi}{2}$ $\qquad\qquad$ $\frac{v}{w_o} > \frac{r}{R}$

$$\varphi = \sin^{-1}\sqrt{\frac{1-r^2/R^2}{1-v^2/w_o^2}} \qquad \frac{v}{w_o} < \frac{r}{R} .$$

$\sigma(r,v)$ is shown in figure 3.

C. MODEL B

We start with expression 18:

$$\frac{dr}{T\, w(\alpha,r)} \frac{3\alpha^2}{R^3} d\alpha .$$

If $d\alpha \gg dr$, then $d\alpha$ corresponds to a range in velocities:

$$w^2 = \omega^2(\alpha^2-r^2) ,$$

$$wdw = \omega^2\alpha d\alpha .$$

In this way the density in $\underline{r}$-$\underline{w}$ space is obtained; expression 18 becomes

$$\frac{3}{T\ \omega^2 R^3}\sqrt{\frac{w^2}{\omega^2} + r^2}\ drdw$$

($\underline{r}$ is the spatial radius). A fraction $\sin\theta\, d\theta$ of the galaxies are contained within a thin cone of angle θ and thickness $d\theta$ (fig. 23). The density of these galaxies in $\underline{v}$-$\underline{r}$ space (from here on, $\underline{r}$ is the projected radius) is

$$\frac{3}{\pi R^3\omega}\sqrt{\frac{v^2\sec^2\theta}{\omega^2} + r^2\csc^2\theta}\ \sec\theta\ \csc\theta\ \sin\theta\ d\theta .$$

The factors $\sec\theta$ and $\csc\theta$ come from changing the coordinates. This density can be integrated to give

$$\sigma = \frac{3}{\pi R^3 \omega}\left[(R-r)\tanh z + rz\right] ,$$

where $$z = \operatorname{sech}^{-1}\left[\frac{|v|}{(R-r)\omega}\right] .$$

σ is shown in figure 4. $\frac{dF}{dr}$ is obtained by integrating σ with respect to $\underline{v}$.

$$F(r) = \frac{1}{2}\frac{r}{R}\left(3 - \frac{r^2}{R^2}\right) .$$

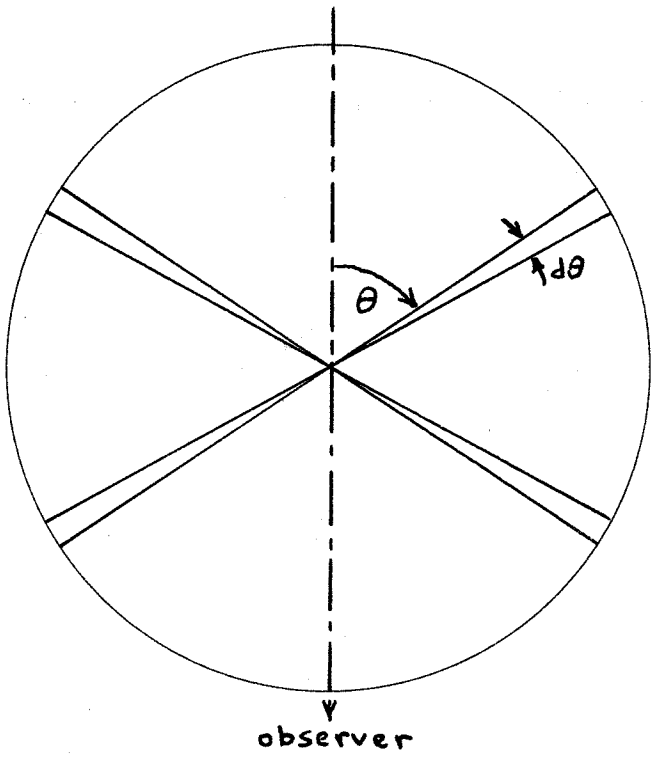

FIGURE 23

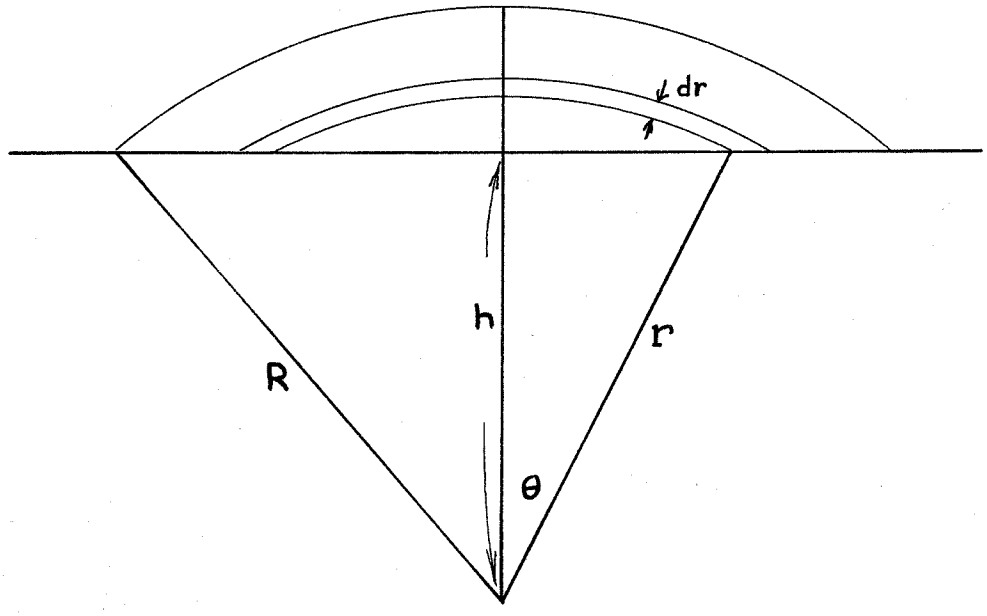

FIGURE 24

APPENDIX II. ABELL'S PLATE FRACTION f

Assuming good centering, Abell's plate cuts off parts of the Coma cluster on each of the four sides of the plate (fig. 24). The fraction of galaxies excluded is the sum of four integrals of the form

$$\int_{r=h}^{r=R} \frac{\theta(r)}{\pi} \frac{dF(r)}{dr}\, dr ,$$

where

$$\theta = \cos^{-1} \frac{h}{r} ,$$

and h takes the values 78' and 81'. Thus

$$1 - f = \frac{2}{\pi}\int_{\theta=0}^{\cos^{-1}\frac{78}{100}} \left[1 - F(78' \sec\theta)\right] d\theta + \frac{2}{\pi}\int_{\theta=0}^{\cos^{-1}\frac{81}{100}} \left[1 - F(81' \sec\theta)\right] d\theta .$$

Numerical computation based on the 48-inch counts yields

$$1-f = 0.058 \pm 0.013 .$$

Model A gives a slightly different value because the model doesn't agree perfectly with the data. In this case there are four spherical caps of cross section shown in figure 24. The fraction of galaxies excluded is the sum of four integrals of the form

$$\int_{r=h}^{R} 2\pi r(r-h)\rho \, dr \ ,$$

where ρ is approximately $\frac{1}{4\pi Rr^2}$. Thus

$$1-f = \int_{78'}^{100'} \left(1 - \frac{78'}{r}\right) \frac{dr}{100'} + \int_{81'}^{100'} \left(1 - \frac{81'}{r}\right) \frac{dr}{100'} \ .$$

$$1-f = 0.042 \ .$$

APPENDIX III. THE SURFACE INTEGRAL $\iint \bar{\sigma}\, r^i w^i w^j d^3w\, dS^j$ FOR A GAS

Choose the x-axis in the direction of the vector dS^j and choose the z-axis perpendicular to both dS^j and r^i. Let θ be the angle between dS^j and r^i. Then

$$r^i w^i = r(w^x \cos\theta + w^y \sin\theta)$$

and

$$w^j dS^j = w^x dS \ .$$

The product of these two expressions is

$$rdS\left[(w^x)^2 \cos\theta + w^x w^y \sin\theta\right].$$

When this is multiplied by $\bar{\sigma}$ and integrated over velocity space, the second term vanishes due to isotropy, and we are left with

$$\tfrac{1}{3}\rho\overline{w^2} rdS \cos\theta$$

or

$$\tfrac{1}{3}\rho\overline{w^2} r^i dS^i \ .$$

APPENDIX IV. METHOD B

The potential $\phi(r)$ satisfies the field equation

$$\frac{1}{r^2}\frac{d}{dr}r^2\frac{d\phi}{dr} = 4\pi G\rho$$

or $$\frac{1}{r}\frac{d^2}{dr^2}(r\phi) = 4\pi G\rho \ .$$

Two integrations give

$$r\,\phi(r) = -4\pi G\int_0^r S(r')dr'$$

where $$S(r) = \int_r^\infty r'\,\rho(r')dr' \ .$$

The potential energy is therefore

$$\frac{M^2}{GR\nu} = \frac{-1}{2}\int_0^\infty 4\pi r^2\phi\rho\,dr = 8\pi^2 G\int_0^\infty \frac{dS}{dr}dr\int_0^r S(r')dr'$$

or $$\frac{M^2}{GR\nu} = 8\pi^2 G\int_0^\infty S^2(r)dr \ .$$

But $$M = 4\pi\int_0^\infty S(r)dr \ .$$

Therefore $$\nu = \frac{2}{R}\,\frac{\left(\int_0^\infty S dr\right)^2}{\int_0^\infty S^2 dr} \ .$$

APPENDIX V. COLLISIONS

Spitzer and Baade[23] calculated the number of collisions a galaxy in the Coma cluster would encounter by traveling for 3×10^9 years through the cluster. This is the time for one traversal in model B. For a galaxy passing through the center, they estimated that the number of collisions would be the order of several hundred. However, the change to the new distance scale reduces this result by a factor 7^{-3} or 0.003.

Model A gives the result easily. The number of collisions undergone by a galaxy of area $\pi \lambda^2$ in crossing the center of the Coma cluster is approximately

$$2 \int_0^{\alpha} \sqrt{2}\, 4\pi \lambda^2 \rho \, dr$$

where $$\rho = \frac{\mathcal{N}}{4\pi R c^2} \qquad 0 < r < c \ ,$$

$$\rho = \frac{\mathcal{N}}{4\pi R r^2} \qquad c < r < R \ .$$

The factor $\sqrt{2}$ is inserted to include the motions of the other galaxies. $\frac{1}{R}$ and $\frac{1}{\alpha}$ are neglected compared to $\frac{1}{c}$. The number of collisions is then the order of

$$\frac{4\sqrt{2}\, \mathcal{N} \lambda^2}{Rc} \ .$$

For $\mathcal{N} = 1560$ $\qquad R = 2.6$ Mpc

$\lambda = 10$ kpc $\qquad c = 0.05\ R$,

there are 3 collisions. If N is 13,000, then there would be around 25 collisions.